PRISM VALIDATION AND APPLICATIONS

Robert E. Daniell, Jr.

Computational Physics, Inc.
207 Fulton Street
Norwood, MA 02062

1 May 2003

Final Report

20031201 022

AIR FORCE RESEARCH LABORATORY
Space Vehicles Directorate
29 Randolph Rd
AIR FORCE MATERIEL COMMAND
HANSCOM AFB, MA 01731-3010

This technical report has been reviewed and is approved for publication.

/Signed/
Contract Manager

/Signed/
Branch Chief

REPORT DOCUMENTATION PAGE

Form Approved
OMB No. 0704-0188

1. AGENCY USE ONLY (*Leave blank*)	2. REPORT DATE 1 May 2003	3. REPORT TYPE AND DATES COVERED Scientific Report No. 2 (12 Jul 99 - 12 Jan 03)

4. TITLE AND SUBTITLE

PRISM Validation and Applications

6. AUTHOR(S)

Robert E. Daniell, Jr.

5. FUNDING NUMBERS

PR – DTRA
TA – BB
WW – SS
Contract F19628-99-C-0068

7. PERFORMING ORGANIZATION NAME(S) AND ADDRESS(ES)

Computational Physics, Inc.
207 Fulton Street
Norwood, MA 02062

8. PERFORMING ORGANIZATION REPORT NUMBER

AFRL-VS-TR-2003-1566

9. SPONSORING / MONITORING AGENCY NAME(S) AND ADDRESS(ES)

Air Force Research Laboratory
29 Randolph Road
Hanscom AFB, MA 01731-3010
Contract Manager: William Borer/VSBXP

10. SPONSORING / MONITORING AGENCY REPORT NUMBER

11. SUPPLEMENTARY NOTES

12A. DISTRIBUTION / AVAILABILITY STATEMENT

Distribution unlimited

12b. DISTRIBUTION CODE

13. ABSTRACT (*Maximum 200 words*)

This report describes PRISM related work performed in two broad areas: Validation and Applications. The Validation effort involved (1) validationg the PRISM topside profile shape using Millstone Hill Incoherent Scatter Radar data, (2) participating in the validation of the HF Propagation code (which includes PRISM) in OpSend, and (3) the initial work on validating PRISM's boundary determination algorithms using DMSP data and tomographic reconstructions from various tomography groups. The Application development effort also involved three separate projects: (1) the development of IREP for calculating ionospheric range and elevation corrections and pulse dispersion from data driven PRISM output in near real time and implementing a demonstration version on an AFRL computer, (2) the initial development of IRDT, an ionospheric radar design tool based on PIM ionospheric climatology, and (3) the development of software to facilitate the use of PRISM for transionospheric range delay and Doppler shift calculations.

14. SUBJECT TERMS

Ionosphere, Data assimilation, Ionospheric specification, Space weather, Nowcasting, Ionospheric radar corrections, Range, Elevation, Pulse dispersion

15. NUMBER OF PAGES
101

16. PRICE CODE

17. SECURITY CLASSIFICATION OF REPORT	18. SECURITY CLASSIFICATION OF THIS PAGE	19. SECURITY CLASSIFICATION OF ABSTRACT	20. LIMITATION OF ABSTRACT
Unclassified	Unclassified	Unclassified	SAR

NSN 7540-01-280-5500

Standard Form 298 (Rev. 2-89)
Prescribed by ANSI Std. Z39-18
298-102

Table of Contents

List of Figures

List of Tables

Executive Summary

This document provides a description of two broad PRISM related efforts undertaken by CPI: Validation and Applications. The Validation effort involved three separate projects: (1) validation of the PRISM topside profile shape using Millstone Hill Incoherent Scatter Radar (ISR) data, (2) providing PRISM runs for use in the validation of the OpSend HF radio propagation product, and (3) a first attempt at validation of the regional boundary determination algorithms in PRISM. The Application effort also involved three separate projects: (1) development of IREP for calculating ionospheric range and elevation corrections and pulse dispersion in near real time from PRISM output, (2) development of a demonstration version of IRDT, a radar design tool for estimating statistical distribution of range error, elevation error, and pulse dispersion for a user specified radar frequency, bandwidth, and location, and (3) an IDL procedure for estimating ionospheric range delay and ionospheric Doppler shift for transionospheric radio propagation.

1. INTRODUCTION

A large part of the work performed by Computational Physics, Inc. (CPI) under this contract was the correction of problems found in Version 1.7 of the Parameterized Real-time Ionospheric Correction Algorithm (PRISM) and implementing certain improvements to the code. These were documented in the Interim Report which incorporates a complete, updated description of the code.

The Final Report concentrates on two additional areas of work performed by CPI: Validation and Applications. The Validation effort encompassed three separate areas (1) validation of the PRISM topside profile shape using Millstone Hill Incoherent Scatter Radar (ISR) data, (2) providing PRISM runs for use in the validation of the OpSend HF radio propagation software, and (3) validation of the regional boundary determination algorithms in PRISM. The first effort verified a suspicion voiced by Dr. Dwight Decker of AFRL that, on average, PRISM overestimates the topside electron density. However, the current data demonstrate that the problem lies specifically with PRISM's topside profile shape in that the topside scale height is too large. The second effort simply involved delivery of PRISM output for specific times so that the OpSend ray tracing code could be applied. The results of this effort have not been communicated to the author. The third effort involved acquisition of DMSP data, reformatting that data for use by PRISM, and the development of specific IDL procedures to facilitate comparison of PRISM output with tomographic reconstruction. Funding ran out before a detailed study of the results could be undertaken, but the software was delivered to AFRL.

The Application effort involved three separate developments: (1) IREP for calculating ionospheric range and elevation corrections and pulse dispersion in near real time from PRISM output, (2) IRDT, a radar design tool for estimating statistical distribution of range error, elevation error, and pulse dispersion for a user specified radar frequency, bandwidth, and location, and (3) an IDL procedure for estimating ionospheric range delay and ionospheric Doppler shift for transionospheric radio propagation applications. The first effort involved developing and implementing a demonstration of the code, which ran for some time on a computer at AFRL producing graphical representations of ionospheric range and elevation corrections and pulse dispersion. The second effort involved (a) the production of a database of PIM output covering all seasons, solar activity levels, and local times, (b) the development of an application to read this database and calculate ionospheric range and elevation corrections and pulse dispersion and accumulate statistics, and (c) the development of an IDL procedure to produce graphic representations of these statistics. A preliminary version of this code has been produced and delivered to AFRL. However, more work needs to be done, including augmenting the PIM database with examples of geomagnetic storms and other extreme ionospheric conditions. Finally, the third application involved developing an IDL procedure for setting up PRISM runs driven by TEC data, calculating ionospheric range delay and ionospheric Doppler shift. It also involved setting up an orbit simulation package to allow testing of the software. Although no analysis of the results in comparison with actual data has been performed, the package is available for use.

2. VALIDATION

Although much of the PRISM validation effort was conducted by AFRL personnel and other contractors, CPI did carry out or participate in three significant validation efforts. The first involved the use of Incoherent Scatter Radar (ISR) data from Millstone Hill. The second involved producing PRISM runs to be used by the University of Massachusetts at Lowell in conjunction with their HF ray tracing code in an effort to validate the HF propagation maps produced by the OpSend system. (Here, I will only describe the PRISM runs since the OpSend validation will presumably be described elsewhere.) The third validation effort involve the comparisons of PRISM runs with tomographic reconstructions by three chains of receivers: the Alaskan chain operated by Northwest Research Associates (NWRA), the Greenland chain operated by the University of Texas at Arlington, and the United Kingdom (UK) chain operated by the University of Aberystwyth in Wales.

2.1 *Incoherent Scatter Radar Data*

Because Dr. Peter Sultan (formerly of AFRL) had used the years 1981, 1991, 1992, and 1998 in a project to validate Defense Meteorological Satellite Program (DMSP) Special Sensor Ions, Electrons, and Scintillation (SSIES) data with Millstone Hill data, I searched those years for suitable electron density profiles (EDPs) to use in validating PRISM's topside profile shape. I identified nine separate Millstone Hill experiments (some of them multi-day) with good quality vertical profiles. Even so, the data contain many "bad" profiles: profiles with unphysical structures or shapes, profiles with too much noise, etc. Therefore, I spent considerable time doing quality control: identifying the parameters that were useful as markers for poor quality profiles. On the advice of John Foster, I used the error estimates for electron temperature (T_e) and ion temperature (T_i) as indicators of the quality of individual electron density (n_e) measurements. Specifically, I eliminated all n_e measurements for which either T_e and T_i have errors exceeding 20 percent. I also eliminated top (bottom) points with n_e greater than n_e at the next lower (higher) points, and the top point or top two points if they lay above missing points.

In addition to quality control of individual density points, I eliminated entire profiles that satisfied certain criteria. Among these were:

(1) profiles taken with certain pulse lengths (448 ms and 320 ms).
(3) profiles whose *lowest* point lies above 200 km.
(4) profiles whose *highest* point lies below 600 km.
(5) profiles obtained during periods with Kp greater than 4.5.
(6) Specific profiles (identified by eye from plots) in the experiment beginning on day 82 of 1998.

This quality control is built into an IDL procedure that (1) produces plots of the accepted profiles, (2) estimates f_oF_2 and h_mF_2, (3) creates pseudo-DISS data files, (4) runs PRISM (with and without the pseudo-DISS data), (4) produces plots of each acceptable profile along with climatological and data-driven PRISM profiles, (5) calculates certain profile parameters, and (6) accumulates statistics for the errors in these parameters. The profile parameters are:

(1) Upper TEC (electron content from h_mF_2 to the highest point on the observed altitude grid).

(2) Lower TEC (electron content from the lowest point on the observed altitude grid to h_mF_2).

(3) Full TEC (Upper TEC + Lower TEC).

(4) Upper Half-width (distance from h_mF_2 *up* to the altitude at which n_e is half of N_mF_2).

(5) Lower Half-width (distance from h_mF_2 *down* to the altitude at which n_e is half of N_mF_2).

(6) Full Width at Half Maximum (FWHM) (Upper Half-width + Lower Half-width).

(7) Electron density at 600 km [n_e(600 km)].

The parameter errors for which statistics are accumulated are the relative mean and RMS errors of each of the seven parameters listed above. All errors are calculated as:

$$Error = (Model - Data)/Data$$

and expressed as a percentage.

The experiments that contributed to the statistics are summarized in Table 1. The solar activity levels (low, moderate, high) were assigned based on sunspot number (SSN):

Low:	$0 \leq SSN < 75$
Moderate:	$75 \leq SSN < 125$
High:	$SSN \geq 125$

The seasons were defined as:

Spring:	days 59-150
Summer:	days 151-242
Fall:	days 243-333
Winter:	days 334-365, 1-58

Table 1. Millstone Hill Experiments that Contributed to the PRISM Profile Validation Statistics

Year	Start Day	End Day	$F_{10.7}$	SSN	ΣKp	Season	Solar Activity Level
1989	65	68	190-204	98-133	24-33	Spring	Moderate
1989	275	278	222-223	167-209	10-20	Fall	High
1991	317	318	180	94	26	Fall	Moderate
1992	27	28	231	187	23	Winter	High
1992	212	218	106-135	53-103	8-33	Summer	Moderate
1998	82	86	108-120	51-59	13-24	Spring	Low
1998	264	265	142	138	13	Fall	High
1998	291	293	117-120	81-96	27-43	Fall	Moderate
1998	326	327	127	47	20	Fall	Low

In Table 2 the experiments are displayed in a matrix of seasons and solar activity levels in order to reveal the spottiness of the coverage in those parameters.

Table 2. Matrix of Seasons and Solar Activity Levels			
	Solar Activity Level		
Season	Low	Moderate	High
Spring	1998-082	1989-065	
Summer		1992-212	
Fall	1998-326	1991-317 1998-291	1989-275 1998-264
Winter			1992-027

The matrix shows that while there were data for all solar activity levels and for all seasons, there were some combinations of season and solar activity that were devoid of data. All-in-all, there were a total of 1402 profiles used, but these were not distributed uniformly over local time, solar activity, or seasons.

Besides solar activity and season, statistics were accumulated on the basis of local time, defined as:

Night: 2000-2359, 0000-0359
Day: 0800-1559
Twilight: 0400-0759, 1600-1959

The number of profiles used in the validation effort for each combination of season, solar activity, and local time is given in the Tables 3 through 7 and graphically in Figure 1.

On the pages following Figure 1, the statistics for selected profile parameters are displayed as bar graphs. Since the climatological statistics are not very meaningful for TEC (due to displacement of h_mF_2) and half-width (because this should be unaffected by the peak adjustments), I have suppressed those figures. However, it is of interest to compare the errors in the climatological and data adjusted values for $n_e(600 \text{ km})$, so I have included the climatological plots for these cases.

[The discussion continues after Figure 13.]

Table 3. All Seasons

Solar Activity	All	Local Time Night	Day	Twilight
All	1402	384	532	486
Low	453	205	138	110
Moderate	218	22	117	79
High	731	157	277	297

Table 4. Spring

Solar Activity	All	Local Time Night	Day	Twilight
All	451	207	130	114
Low	381	198	94	89
Moderate	70	9	36	25
High	0	0	0	0

Table 5. Summer

Solar Activity	All	Local Time Night	Day	Twilight
All	38	0	24	14
Low	0	0	0	0
Moderate	38	0	24	14
High	0	0	0	0

Table 6. Fall

Solar Activity	All	Local Time Night	Day	Twilight
All	867	173	353	341
Low	72	7	44	21
Moderate	110	13	57	40
High	685	153	252	280

Table 7. Winter

Solar Activity	All	Local Time Night	Day	Twilight
All	46	4	25	17
Low	0	0	0	0
Moderate	0	0	0	0
High	46	4	25	17
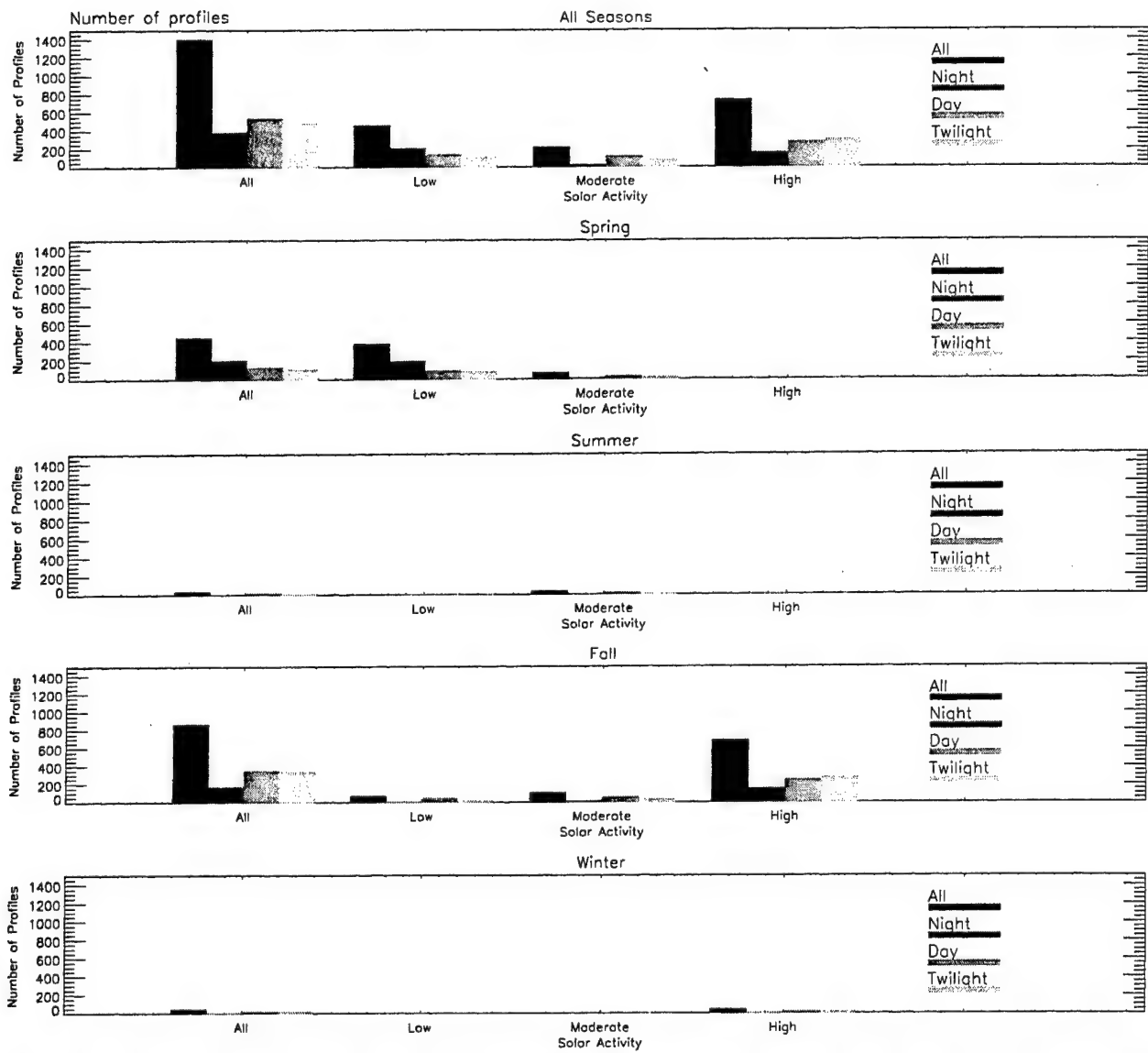
Figure 1. Number of Profiles Used for Each Combination of Season, Solar Activity, and Local Time. Clearly, the statistics for Summer and Winter are somewhat shaky due to the small number of profiles. Also, high solar activity statistics are shaky except during the Fall.
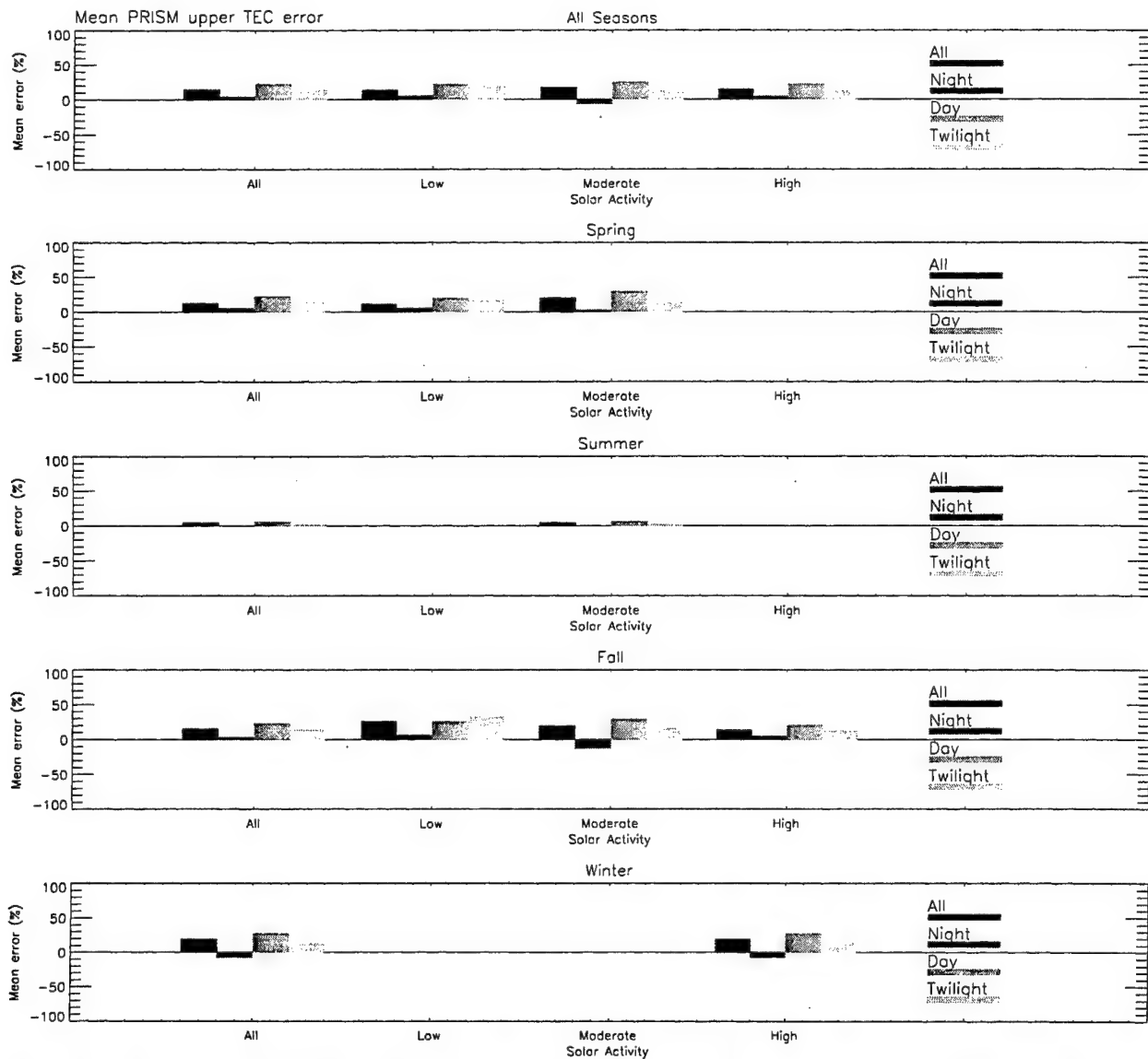
Figure 2. Mean Upper TEC Error for Each Combination of Season, Solar Activity, and Local Time. Note that overall there is a positive bias, meaning that PRISM tends to overestimate the topside TEC. Note also that this positive bias is more pronounced during daytime conditions than at night, when the bias is even negative under some circumstances.
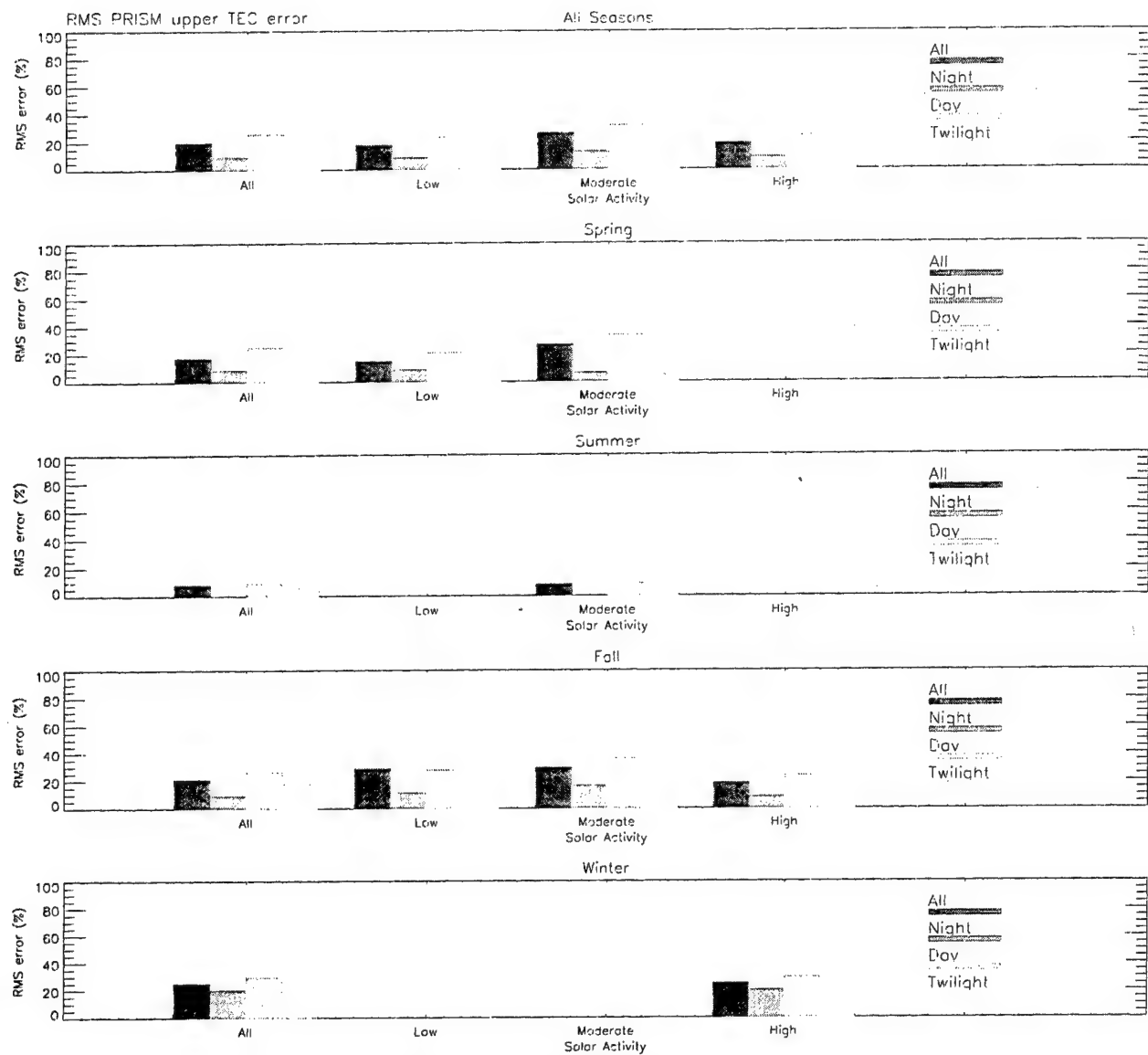
Figure 3. RMS Upper TEC Error for Each Combination of Season, Solar Activity, and Local Time. Note that the RMS error is greatest during the daytime, consistent with the positive bias displayed by the mean error.
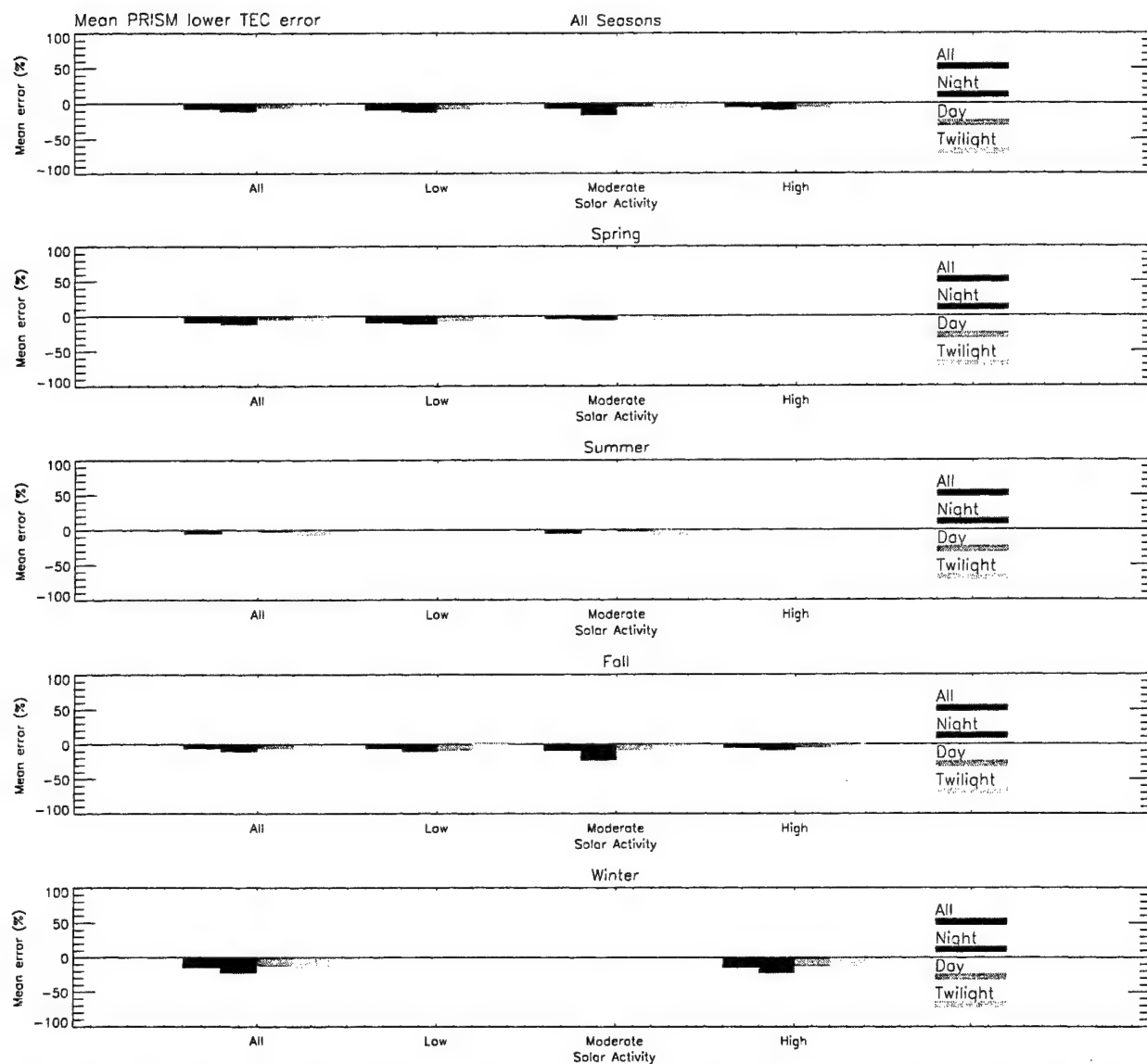
Figure 4. Mean Lower TEC Error for Each Combination of Season, Solar Activity, and Local Time. Note that there is a small negative bias, meaning that PRISM tends to underestimate the bottomside TEC. Although this bias tends to be larger at night than during the daytime, the difference is not as great as for topside TEC.
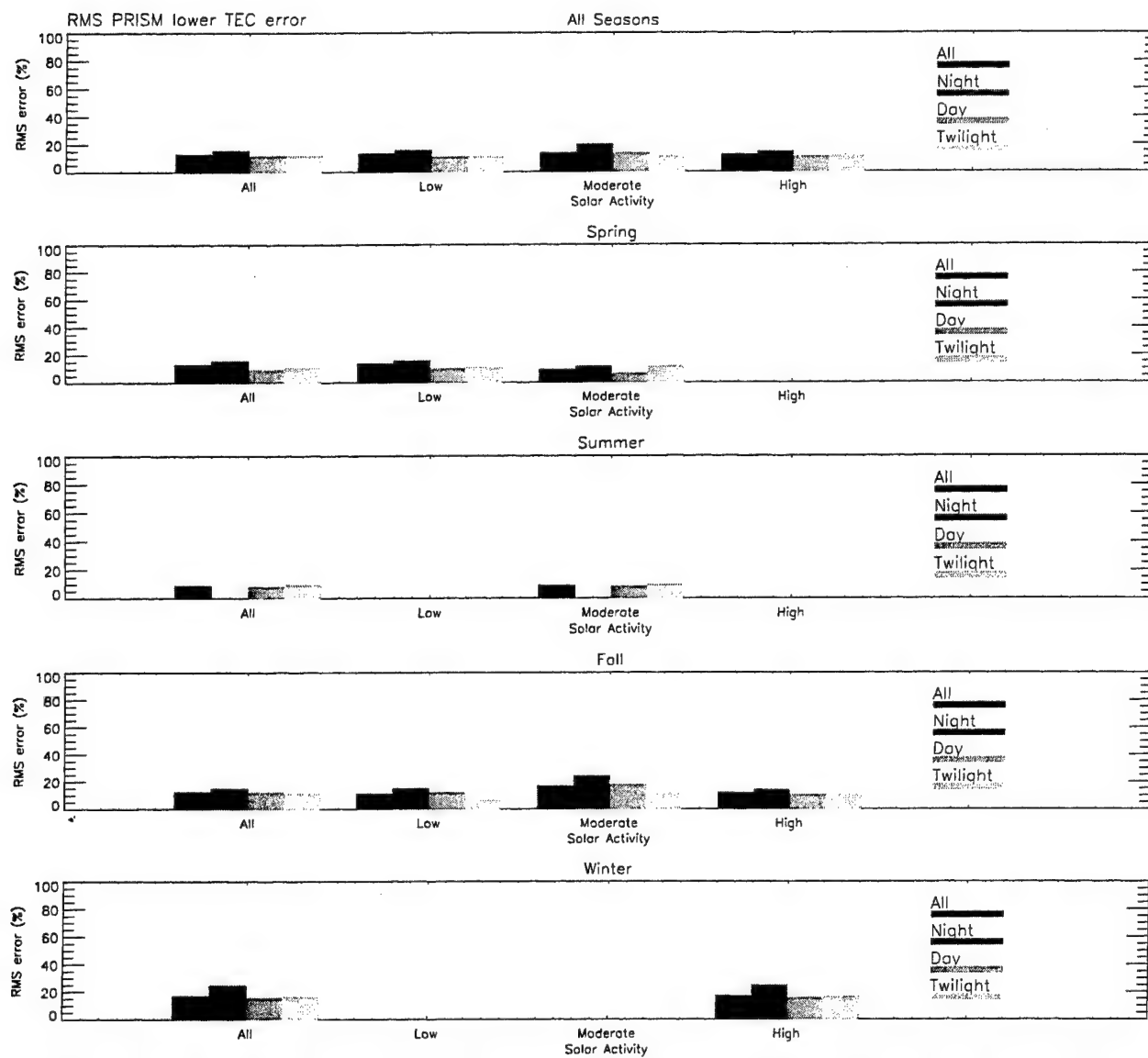
Figure 5. RMS Lower TEC Error for Each Combination of Season, Solar Activity, and Local Time. The RMS error tends to be higher at night then the daytime, although the difference is not as dramatic as for topside TEC.
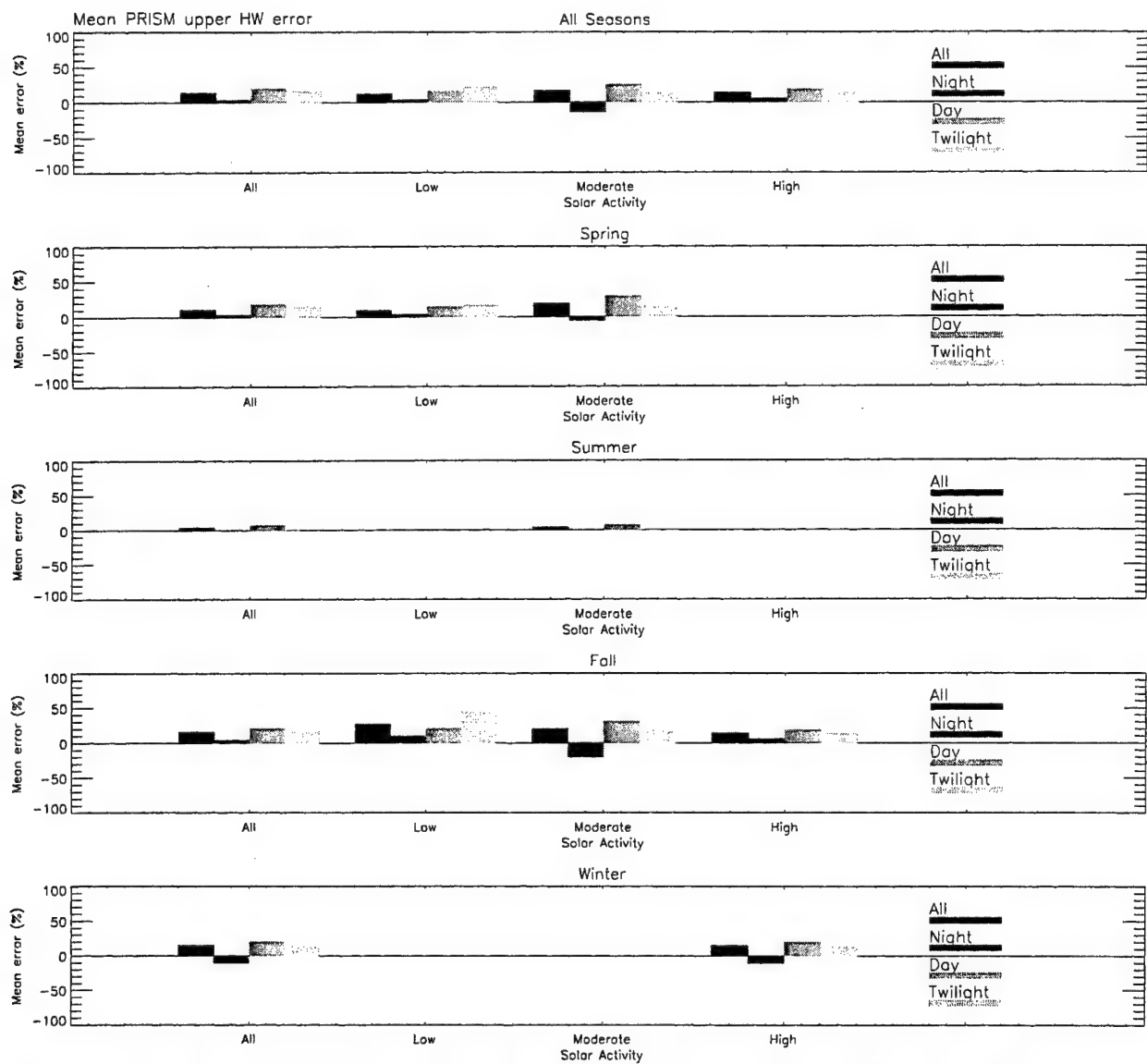
Figure 6. Mean Upper Half-Width Error for Each Combination of Season, Solar Activity, and Local Time. As for topside TEC, there is a positive bias, especially during daytime. The nighttime bias is quite variable, and is quite small overall.

11
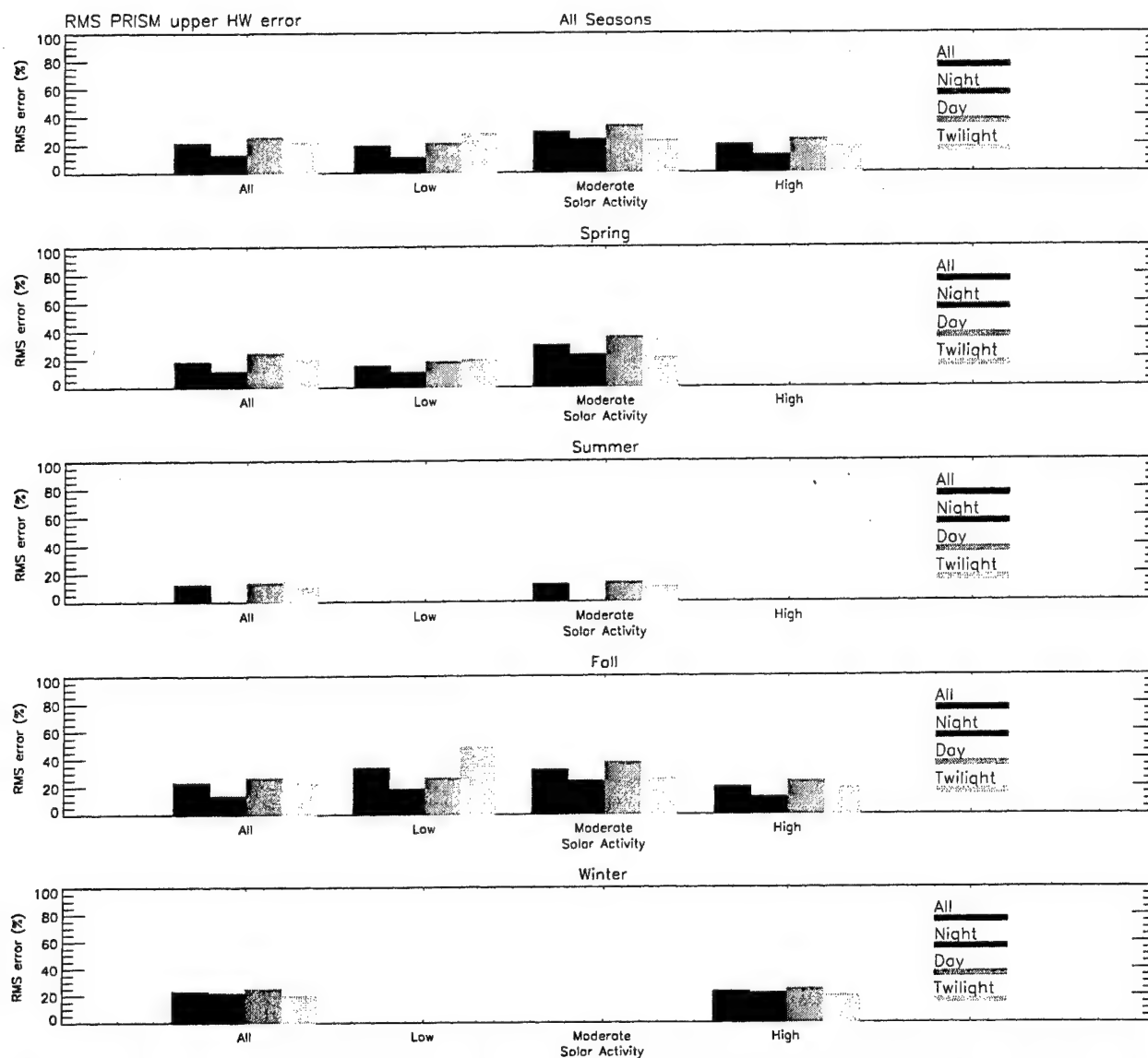
Figure 7. RMS Upper Half-Width Error for Each Combination of Season, Solar Activity, and Local Time. The RMS error is greater during daytime, but not dramatically so, indicating that although that the small nighttime bias is not entirely due to small errors but rather to offsetting positive and negative errors.
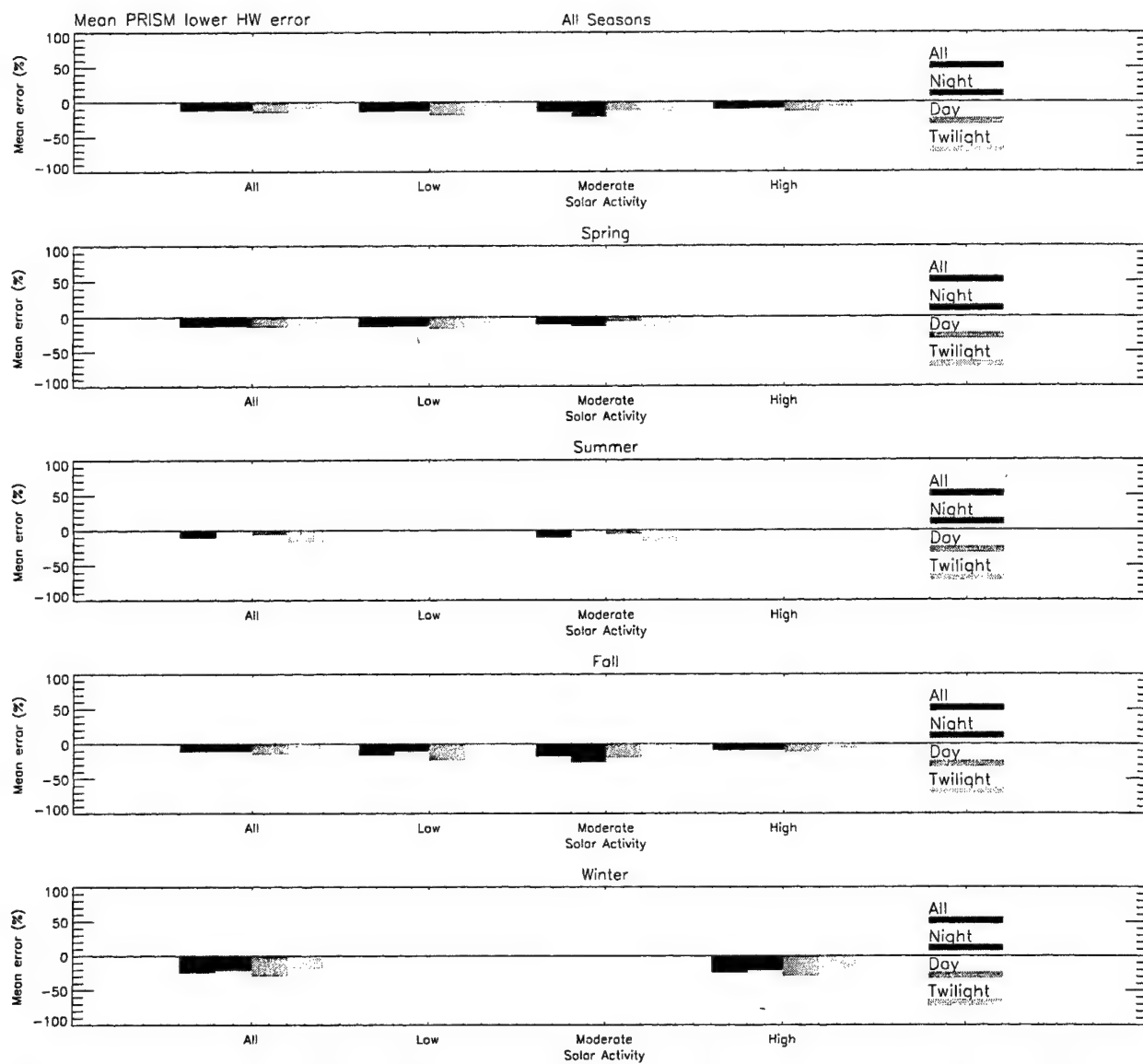
Figure 8. Mean Lower Half-Width Error for Each Combination of Season, Solar Activity, and Local Time. As expected from the behavior of the bottomside TEC, the bottomside half-width also displays a generally negative bias with very little difference between day and night.
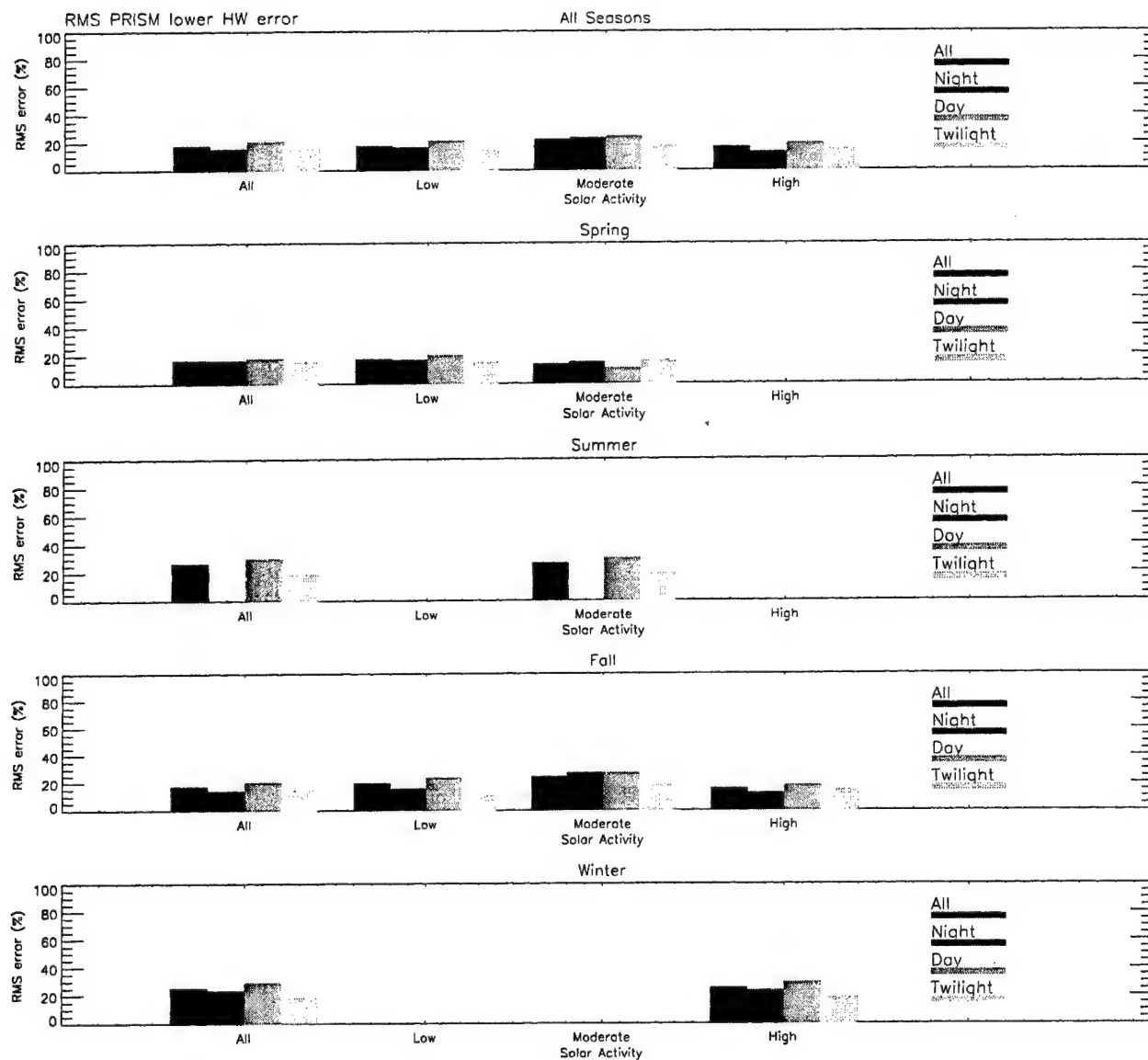
Figure 9. RMS Lower Half-Width Error for Each Combination of Season, Solar Activity, and Local Time. The general lack of significant differences between day and night is consistent with the behavior of the mean error.

14
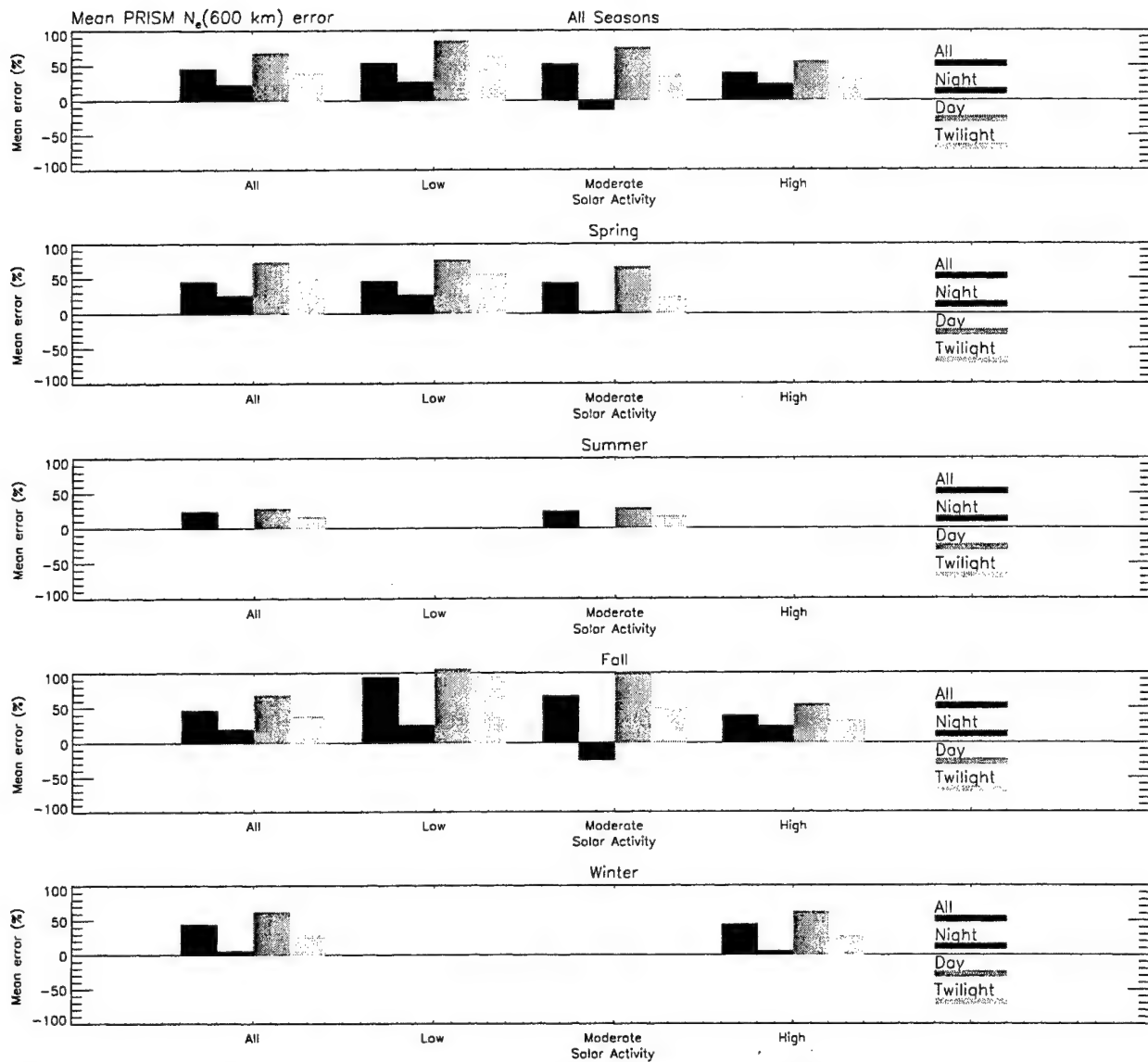
Figure 10. Mean n_e(600 km) Error for Each Combination of Season, Solar Activity, and Local Time. As we would expect from the behavior of the topside TEC and Half-Width, the error in the 600 km electron density displays an overall positive bias with the daytime being always positive while the nighttime is sometimes negative.

15
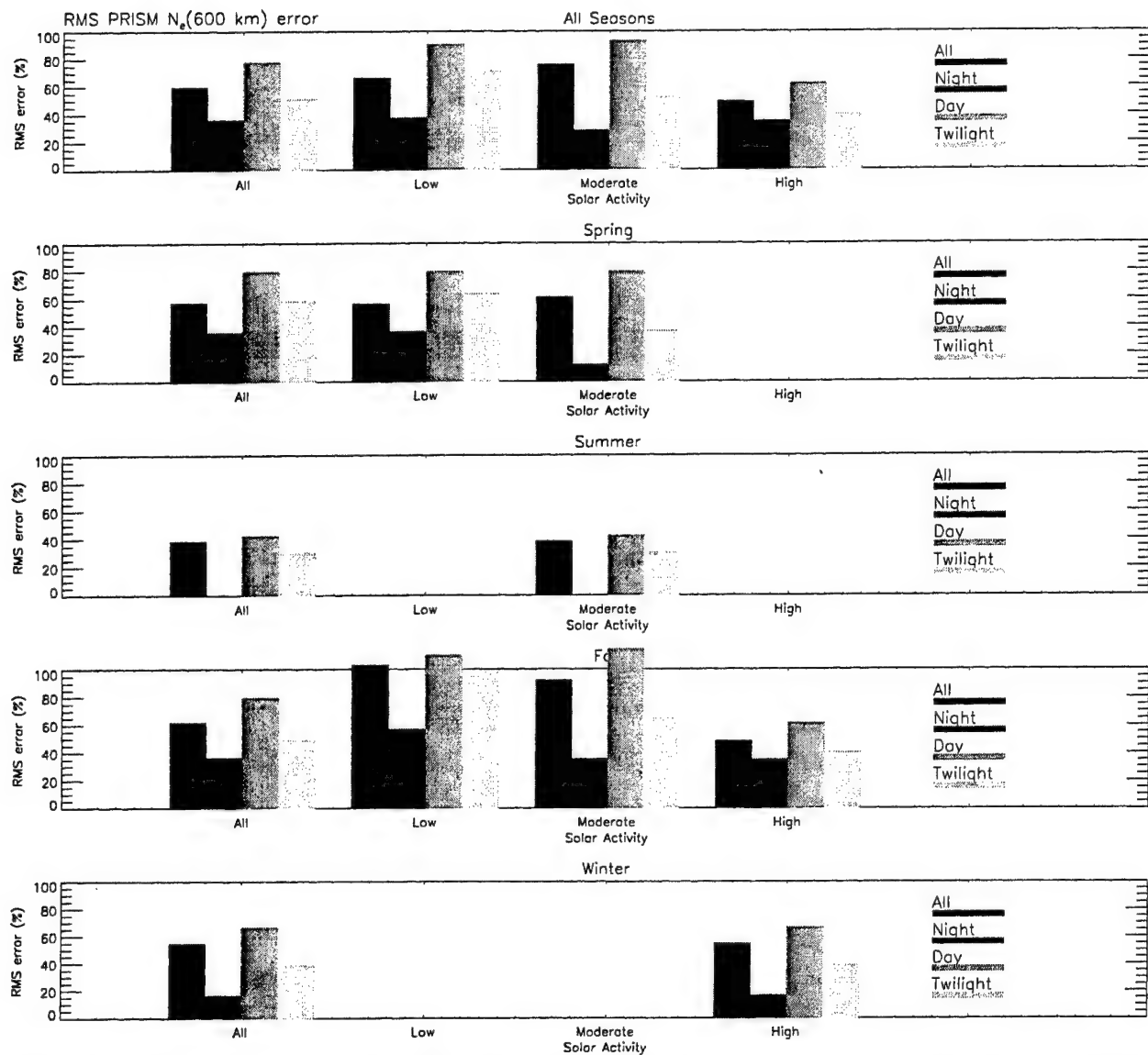
Figure 11. RMS n_e(600 km) Error for Each Combination of Season, Solar Activity, and Local Time. The relative RMS error tends to be considerably larger than the topside TEC and Half-Width errors, as is to be expected due to the exponential fall off of the electron density above the peak. As expected from the behavior of day vs. night errors in topside TEC and Half-Width, the nighttime RMS error at 600 km is smaller than the comparable daytime error.
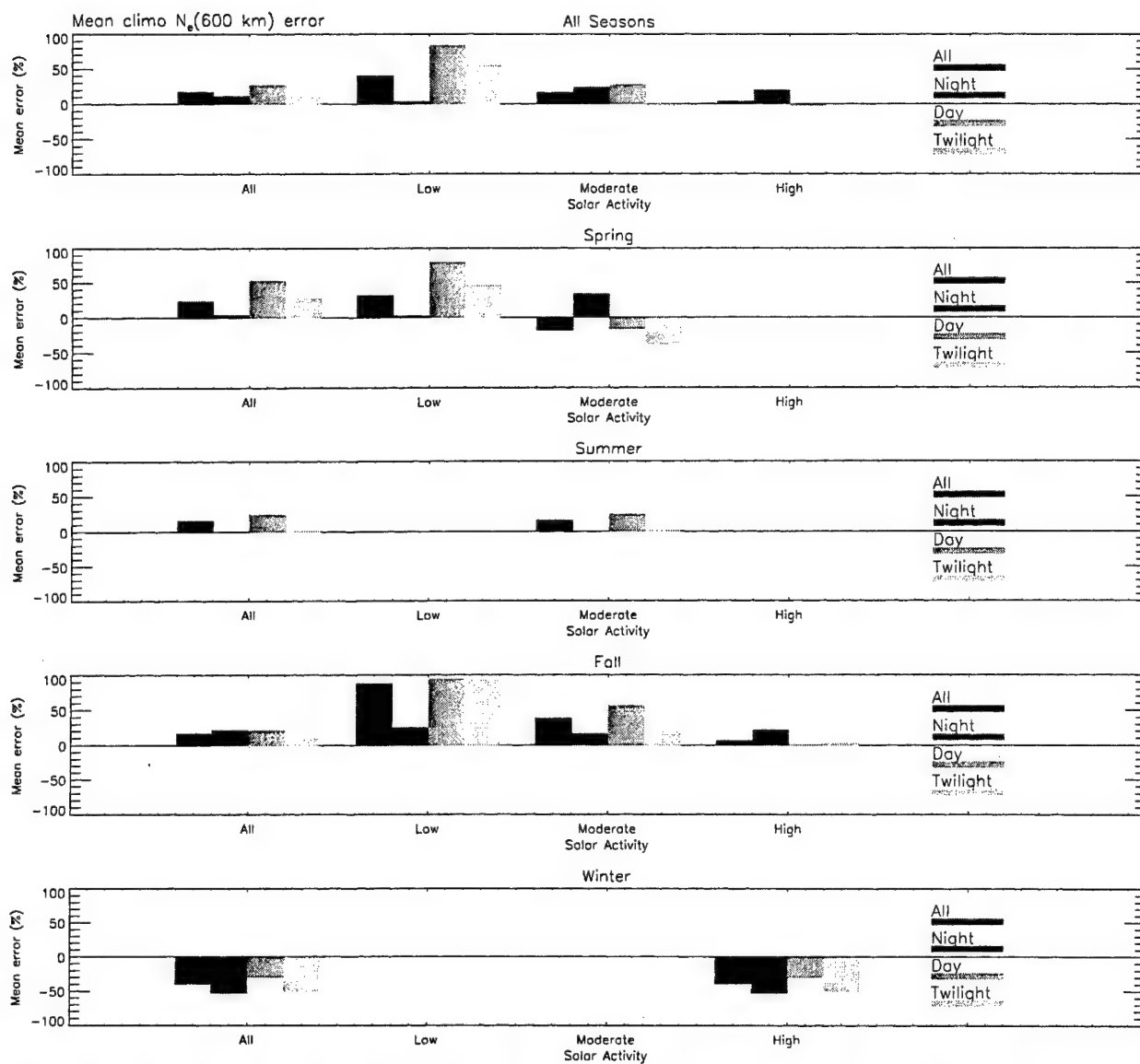
Figure 12. Mean Climatological n_e(600 km) Error for Each Combination of Season, Solar Activity, and Local Time. Although the overall bias is positive (but very small at night) the climatological error shows considerably more variability than the corresponding PRISM error. The winter bias is negative for all local times (although that is based on a miniscule number of profiles).
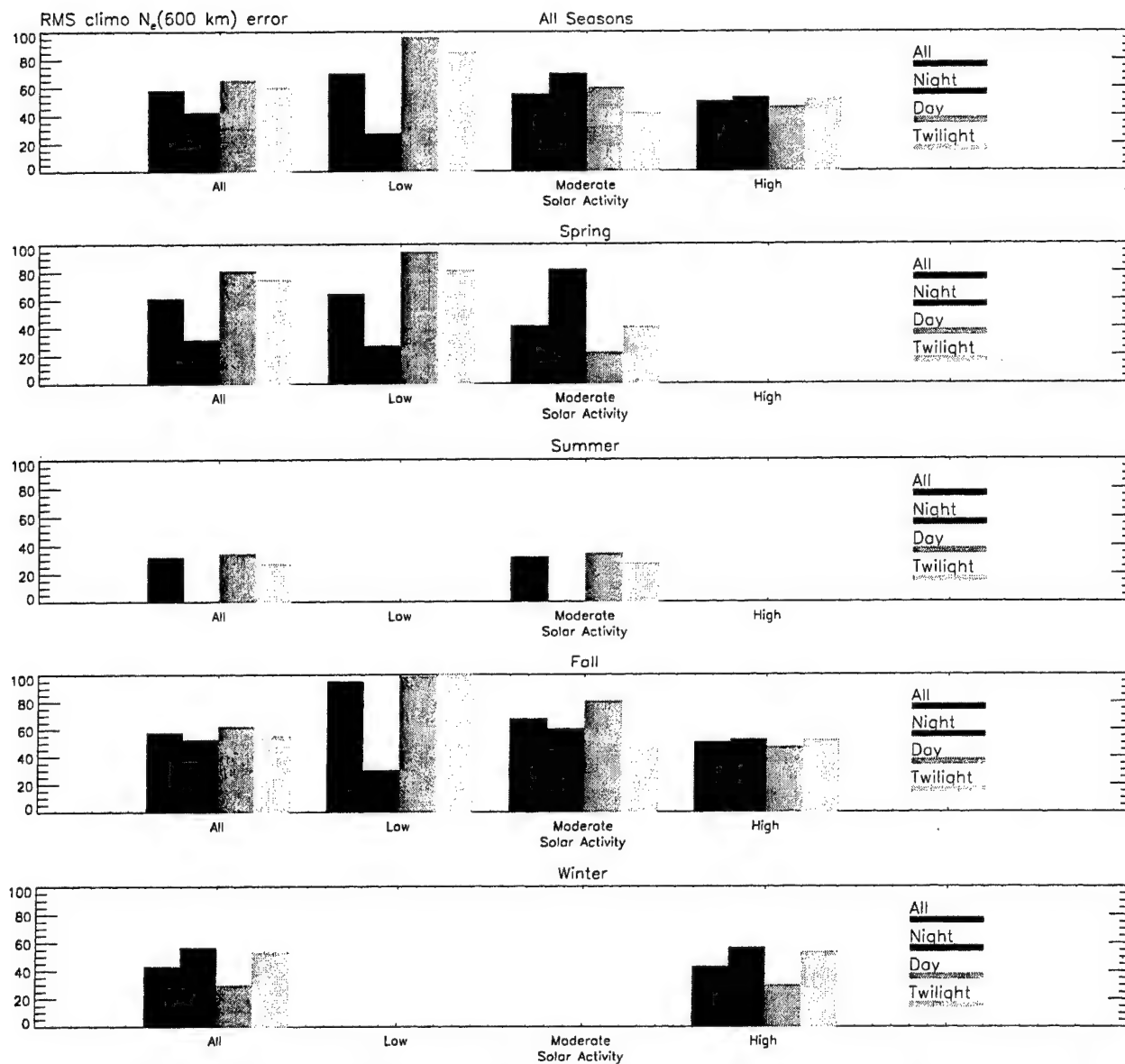
Figure 13. RMS Climatological n_e(600 km) Error for Each Combination of Season, Solar Activity, and Local Time. Interestingly, the climatological RMS error, although still large, tends to be somewhat smaller than the corresponding PRISM error.

18

Discussion

The behavior of the PRISM errors reported here is consistent with Dwight Decker's observation that PIM overestimates the electron density at DMSP altitudes (nominally 840 km). However, the current data demonstrate that the problem lies specifically with PRISM's topside profile shape. The fact that even with the peak adjusted to match the peak parameters measured by the radar, PRISM overestimates all three topside parameters, indicates that PRISM's topside scale height is too large as illustrated in Figure 14.
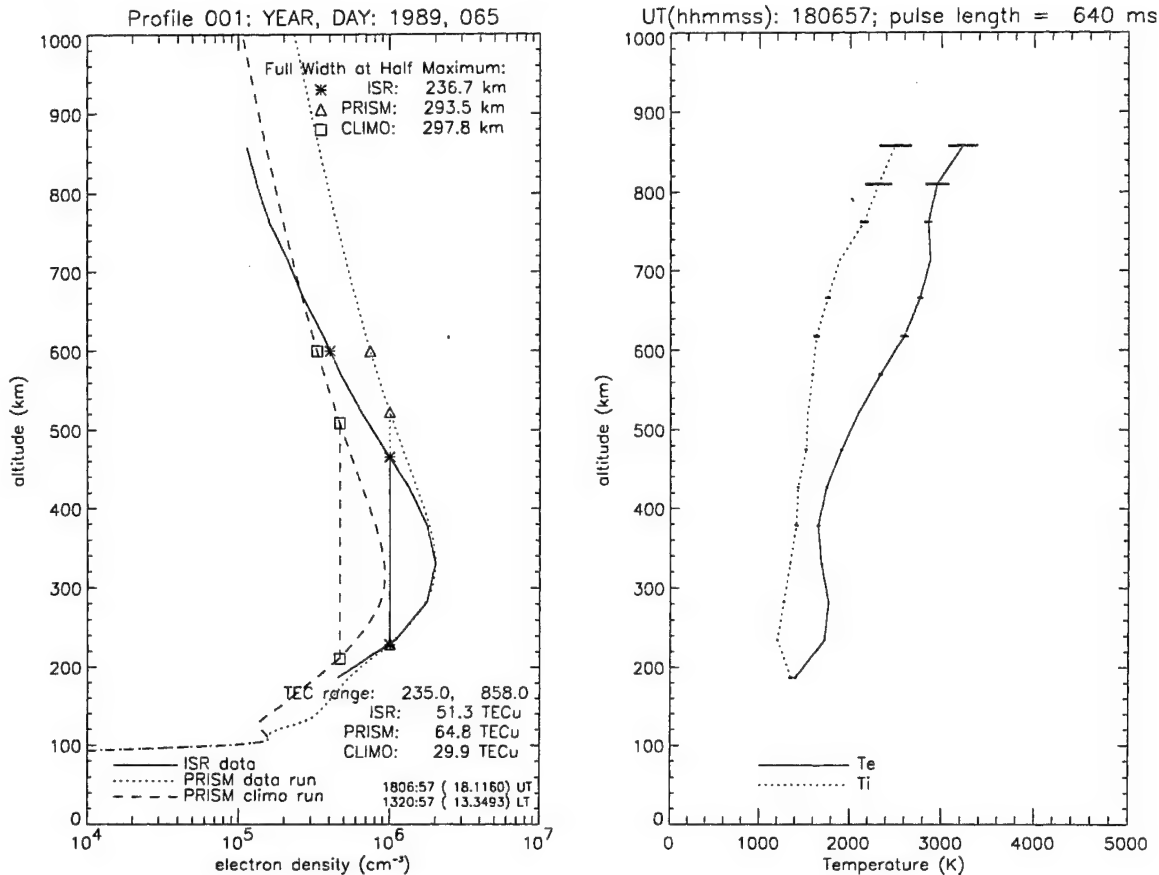
Figure 14. Example of a Daytime Profile for Which PRISM Overestimates the Topside Parameters. Even though the peak has been adjusted to fit the measured values, climatological n_e(600 km) is actually closer to the measured value than the data driven PRISM value due to PRISM's topside scale height being much too large.

The ultimate solution to this problem would be a complete reparameterization of PRISM using state-of-the-art physical models calibrated to reproduce climatological data, including DMSP data. If properly done, this would permit a number of other problems to be corrected, as well as enhancement of PRISM performance. Until such a project is funded, however, Dwight Decker has suggested that a short term solution would be to supplement real-time data with climatological SSIES data. This would require minimal (if any) changes to PRISM while forcing PRISM to adjust its nominal topside scale height downward. The Millstone Hill data obtained for this project, supplemented by additional data to fill in the season/solar activity gaps, would be useful to test and validate this scheme.

2.3 *HF Propagation Validation*

In order to support an effort directed by Dr. Terrence Bullett of AFRL to validate the HF propagation maps produced by the OpSend software package, I made a number of PRISM runs using both Digisonde data provided by Dr. Bullett and DMSP data provided by Dr. Frederick Rich (also of AFRL). These data were for 21-23 September 2000 (Julian days 265-267). The Digisonde data were provided in PRISM compatible format, but the DMSP data had to be reformatted for ingestion by PRISM.

Dr. Rich provided data from the DMSP SSJ/4 instrument and the DMSP SSIES instrument data. The DMSP data was provided as 4 second averages in a dozen files:

```
j1200265.txt, j1200266.txt, j1200267.txt
j1300265.txt, j1300266.txt, j1300267.txt
j1400265.txt, j1400266.txt, j1400267.txt
j1500265.txt, j1500266.txt, j1500267.txt
```

The initial "j" indicates SSJ/4 data, the next two digits (12, 13, 14, or 15) indicated the DMSP satellite number, the meaning of the next two digits are unknown to me, and the next three digits (265, 266, or 267) indicate the Julian day number.

I concatenated these files using the 4NT commands.

```
copy j1200265.txt+j1200266.txt+j1200267.txt f12_js2000265-267.txt
copy j1300265.txt+j1300266.txt+j1300267.txt f13_js2000265-267.txt
copy j1400265.txt+j1400266.txt+j1400267.txt f14_js2000265-267.txt
copy j1500265.txt+j1500266.txt+j1500267.txt f15_js2000265-267.txt
```

These files contain ephemeris information for each 4 second measurement set. Unfortunately, the 110 km coordinates are corrected geomagnetic (CGM) rather than geographic. Therefore, I had to write and run the code "ReadSSJ4" to convert the CGM coordinates at 110 km to geographic coordinates at 110 km. The resulting filenames are:

```
f12_js2000265-267.dat
f13_js2000265-267.dat
f14_js2000265-267.dat
f15_js2000265-267.dat
```

SSIES data:

Provided as 4 second averages by Fred Rich:
```
f12rp00sep21.txt   f12rp00sep22.txt   f12rp00sep23.txt
f13rp00sep21.txt   f13rp00sep22.txt   f13rp00sep23.txt
f14rp00sep21.txt   f14rp00sep22.txt   f14rp00sep23.txt
f15rp00sep21.txt   f15rp00sep22.txt   f15rp00sep23.txt
```

which I stored in D:\data\DMSP\2000_265-267

I concatenated these files using the 4NT commands.

20

```
copy f12rp00sep21.txt+f12rp00sep22.txt+f12rp00sep23.txt f12_rp2000265-267.txt
copy f13rp00sep21.txt+f13rp00sep22.txt+f13rp00sep23.txt f13_rp2000265-267.txt
copy f14rp00sep21.txt+f14rp00sep22.txt+f14rp00sep23.txt f14_rp2000265-267.txt
copy f15rp00sep21.txt+f15rp00sep22.txt+f15rp00sep23.txt f15_rp2000265-267.txt
```

but then I had to delete the 2 header label lines at the beginning of the concatenated sections.

```
S/C YR JDAY HOUR MIN GLAT GLNG GMLATSS MLT110 GMLNGSS GLATSUBSOL …
ALTSTRT ALTEND BN BE BD XECI YECI ZECI POTFLAG APT_POT POT_ION …
```

I made three complete sets of PRISM runs: (1) climatology, with no driver data, (2) DISS data only, and (3) DISS and DMSP data. The results were delivered to Dr. Gary Sales at the University of Massachusetts at Lowell in mid-February 2002.

2.4 *Tomography*

The goal of this effort was to make comparisons between PRISM output and tomographic reconstructions of the ionosphere. Data from a coordinated set of runs were provided by three tomography groups: (1) Northwest Research Associates (NWRA), who provided tomographic reconstructions from their Alaskan (AK) chain, (2) the Applied Research Laboratories (ARL) of the University of Texas at Austin, who provided tomographic reconstructions from their Greenland (GL) chain, and (3) the University of Wales at Aberystwyth, who provided tomographic reconstructions from their chains in the United Kingdom (UK) and the Arctic (AR). All three organizations supplied reconstructions in graphical form for two periods: 19-20 September 2001 and 12-13 December 2001. NWRA provided five ionospheric reconstructions for the September dates and three for the December dates. ARL provided 38 reconstructions for the September dates and 23 reconstructions for 12 December (none for 13 December). Wales provided three reconstructions from each of their chains for 19 September and for 12 December. Tables 8 and 9 detail the reconstructions available for the two sets of dates.

For the sake of brevity I will show only a few representative cases, specifically one each for the AK, GL, and UK chains. The purpose of these initial runs was to investigate PRISM's ability to properly place latitude region boundaries based on DMSP data alone. The DMSP data was provided by Dr. Frederick Rich of AFRL. He supplied data from the SSIES Drift Meter, Retarding Potential Analyzer, and the J/4 energetic particle detector.

The Drift Meter supplies PRISM with the ion drift velocity component perpendicular to the satellite motion, which PRISM attempts to use to identify the equatorward edge of the midlatitude (or subauroral) trough. The Retarding Potential Analyzer provides PRISM with *in situ* ion density and composition as well as Ion temperature (T_i). Because Langmuir Probe data was not supplied, the electron temperature (T_e) was not available. However, PRISM uses the plasma temperature $(T_p = T_i + T_e)$ to set the scale height in the midlatitude region and does not use it to detect any boundaries (although perhaps in a future version it will use it to detect the

21

Table 8: 19-20 September 2001 (Days 262-263)		
Day	UT	Organization/Chain
262	0029	ARL/GL
	0050	ARL/GL
	0331	ARL/GL
	0524	Wales/UK
	0616	ARL/GL
	0703	ARL/GL
	0729	Wales/UK
	0800	ARL/GL
	0852	ARL/GL
	0917	ARL/GL
	1033	Wales/UK
	1106	ARL/GL
	1212	ARL/GL
	1306	ARL/GL
	1400	ARL/GL
	1608	ARL/GL
	1624	Wales/Arctic
	1632	NWRA/AK
	1836	Wales/Arctic
	1900	ARL/GL
	1951	ARL/GL
	2022	ARL/GL
	2047	ARL/GL
	2131	Wales/Arctic
	2212	ARL/GL
263	0000	ARL/GL
	0058	ARL/GL
	0152	ARL/GL
	0213	NWRA/AK
	0245	ARL/GL
	0521	NWRA/AK
	0556	ARL/GL
	0622	ARL/GL
	0716	ARL/GL
	0807	ARL/GL
	0841	ARL/GL
	0904	ARL/GL
	1030	ARL/GL
	1037	ARL/GL
	1130	ARL/GL
	1314	ARL/GL
	1410	ARL/GL
	1428	NWRA/AK
	1503	ARL/GL
	1556	NWRA/AK
	1815	ARL/GL
	2004	ARL/GL
	2144	ARL/GL
	2331	ARL/GL

Table 9: 12-13 December 2001 (Days 346-347)		
Day	UT	Organization/Chain
346	0131	ARL/GL
	0318	ARL/GL
	0350	ARL/GL
	0404	ARL/GL
	0537	ARL/GL
	0629	ARL/GL
	0640	ARL/GL
	0654	ARL/GL
	0816	ARL/GL
	0839	ARL/GL
	1006	ARL/GL
	1103	NWRA/AK
	1400	NWRA/AK
	1418	ARL/GL
	1500	ARL/GL
	1637	ARL/GL
	1644	ARL/GL
	1659	ARL/GL
	1836	ARL/GL
	1913	ARL/GL
	1938	ARL/GL
	2058	ARL/GL
	2047	ARL/GL
	2126	ARL/GL
347	0049	ARL/GL
	0150	Wales/UK
	0235	ARL/GL
	0247	NWRA/AK
	1158	Wales/UK
	1256	Wales/Arctic
	1445	
	1522	Wales/Arctic
	1626	ARL/GL
	0715	Wales/UK

trough). Thus, the lack of temperature data is not a serious omission. The J/4 data is used by PRISM to set the equatorward and poleward edges of the auroral oval.

The figures on the following pages (Figures 15, 16, and 17) are simply intended to give a flavor of the capabilities of the software. The original figures are in color, but are reproduced here in black and white to avoid the expense and complication of color reproduction. A study of the implications of the results will have to come from a future effort.

Figure 15. A Comparison Between the Tomographic Reconstruction From the NWRA AK Chain at 1433 UT on 20 September 2001 With a PRISM Run for the Same Date and Time. Only DMSP SSIES and SSJ/4 data were ingested by PRISM.

Figure 16. A Comparison Between the Tomographic Reconstruction From the ARL GL chain at 0029 UT on 19 September 2001 With a PRISM Run for the Same Date and Time. Only DMSP SSIES and SSJ/4 data were ingested by PRISM.
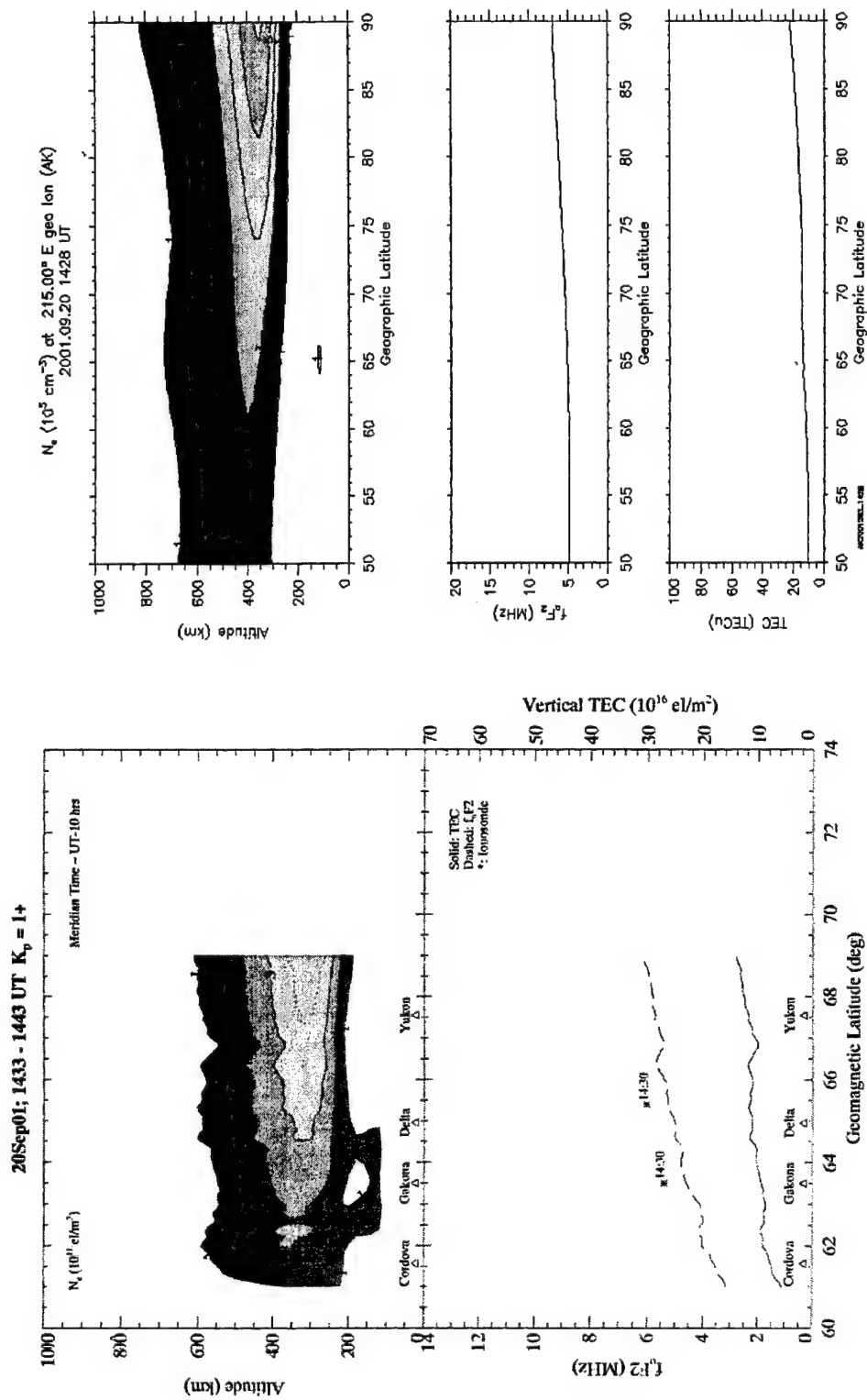
Figure 17. A Comparison Between the Tomographic Reconstruction From the University of Wales UK Chain at 2131 UT on 19 September 2001 With a PRISM Run for the Same Date and Time. Only DMSP SSIES and SSJ/4 data were ingested by PRISM.
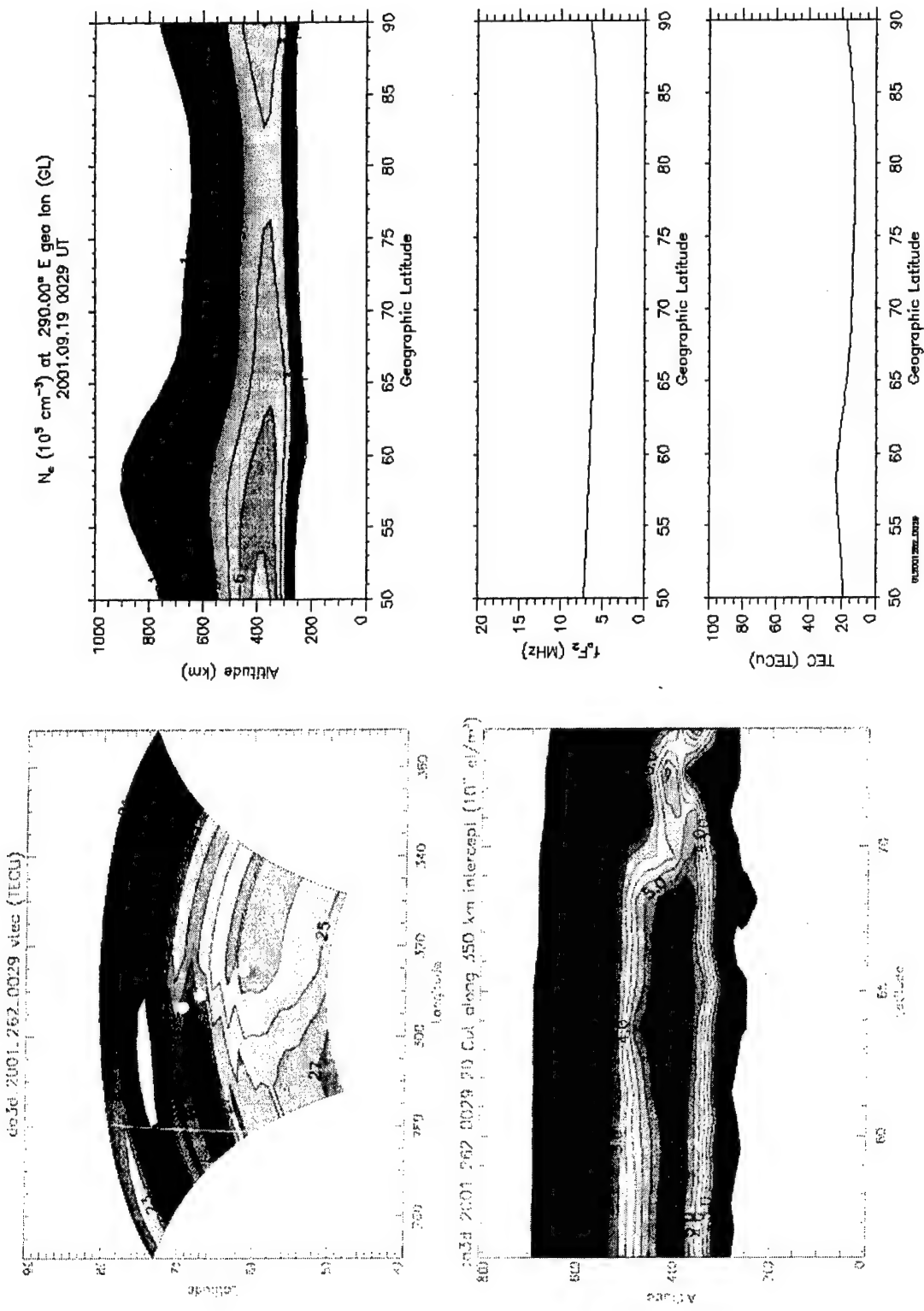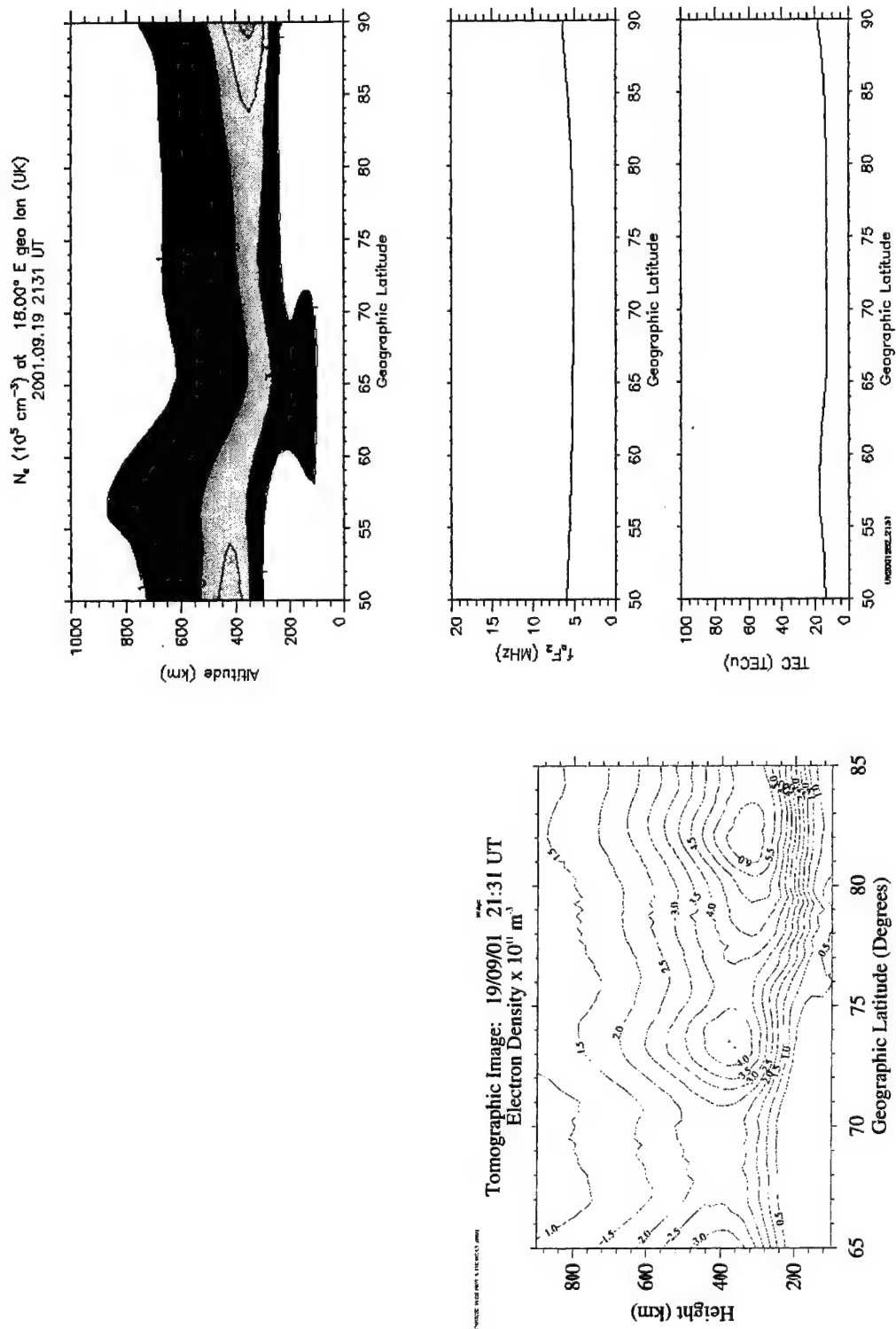
3. APPLICATIONS

In addition to participating in various PRISM validation activities, I also developed two PRISM applications related to ionospheric effects on radar signals, and along with Ray Barnes, investigated the use of PRISM for transionospheric radio propagation calculations.

3.1 *IREP*

The first PRISM application was developed at the request of, and with the support of, Mr. Greg Bishop of AFRL. It was designed to calculate ionospheric range and elevation corrections and pulse dispersion (hence IREP = Ionospheric Range, Elevation, and Pulse dispersion) by ray tracing through PRISM output. It is derived from the Ionospheric Error Correction Model (IECM) that was developed by CPI under an SBIR subcontract to Research Associates of Syracuse (RAS) for operational use at the ALTAIR radar located at the Army's Kwajalein Missile Range.

IREP consists of four major components: (1) a FORTRAN code to produce the desired radar corrections, (2) an IDL procedure to produce graphical output of those corrections, (3) a script to control the running of the two codes in real time, and (4) a set of control files that permits the user to tailor the output and displays to his or her particular situation.

The IREP FORTRAN code: (a) reads the control files to determine the radar characteristics and the output grid parameters, (b) reads a PRISM output file and converts it from electron density on a latitude/longitude/altitude grid to integrated electron content on a range/azimuth/elevation grid (an Electron Content Model or ECM), (c) calculates range corrections, elevation corrections, and pulse dispersion on that same range/azimuth/elevation grid, and (d) writes the results to the IREP specification file.

An example of the radar characteristics file, called "radarfreq.dat" is shown in Figure 18. The IREP FORTRAN module only uses the frequency information. The remaining two lines are for use by the IDL procedure. The output grid is specified in the file "radargrid.in", an example of which is displayed in Figure 19. Note that IREP (like IECM before it) uses an elevation

```
2                  = NFREQ, the number of radar frequency pairs
396.0   404.0      = lower limit, upper limit of pulse bandwidth
990.0 1010.0       = lower limit, upper limit of pulse bandwidth
A                  = "A" for constant altitude, "R" for constant range
20000.0            = altitude or range for display
```

Figure 18. An Example of the Format of the IREP Input File "radarfreq.dat". This file is used both by the FORTRAN module and the IDL module. In this example only 2 radar frequency ranges are specified, but any number are permitted. Also, the display is specified to be at a constant altitude of 20,000 km. (The display information is ignored by the FORTRAN module.) The comments (following the equal signs) are intended to make the file more readable, but are ignored by the both the FORTRAN module and the IDL procedure.

dependent range grid that takes into account the horizontal stratification of the ionosphere.

```
 25.0, 50.00  :site coords: lat (deg N) REAL[-90.0,90.0], lon (degrees E) REAL[0.0,360.0)
   20      :Number of elevations INTEGER>0; followed by Elevation grid (deg)   REAL[0.0,90.0]
  0.01  1.00  2.00  3.00  4.00  5.00  6.00  7.00  8.00  9.00 10.00 12.00 14.00
 17.00 20.00 25.00 30.00 40.00 60.00 89.99
   37      :Number of azimuths INTEGER>0; followed by Azimuth grid (deg) REAL[0.0,360.0]
   0.00  10.00  20.00  30.00  40.00  50.00  60.00  70.00  80.00  90.00
 100.00 110.00 120.00 130.00 140.00 150.00 160.00 170.00 180.00 190.00
 200.00 210.00 220.00 230.00 240.00 250.00 260.00 270.00 280.00 290.00
 300.00 310.00 320.00 330.00 340.00 350.00 360.00
   67      :Number of altitudes INTEGER[1,1000]; followed by Alt grid (km)   REAL[90.0,25000.0]
   90.00   100.00   125.00   150.00   175.00   200.00   210.00   220.00
  230.00   240.00   250.00   260.00   270.00   280.00   290.00   300.00
  310.00   320.00   330.00   340.00   350.00   360.00   370.00   380.00
  390.00   400.00   410.00   420.00   430.00   440.00   450.00   460.00
  470.00   480.00   490.00   500.00   525.00   550.00   575.00   600.00
  625.00   650.00   675.00   700.00   750.00   800.00   850.00   900.00
  950.00  1000.00  1100.00  1200.00  1300.00  1400.00  1500.00  2000.00
 3000.00  4000.00  5000.00  7500.00 10000.00 12500.00 15000.00 17500.00
20000.00 22500.00 25000.00
```

Figure 19. An Example of the Grid Control File "radargrid.in" That Tells the IREP FORTRAN Module How to Organize the Output. Note the specification of *altitudes* rather than *ranges*, resulting in an elevation dependent range grid. This is done because the ionosphere is horizontally stratified.

The range and elevation errors are calculated in the FORTRAN module by performing a two-dimensional ray trace through the ECM and comparing the true range and elevation with the apparent range and elevation:

$$\Delta R\left(R_{app}, A, E_{app}; f\right) = R_{app}\left(R_{app}, A, E_{app}; f\right) - R_{true}\left(R_{app}, A, E_{app}; f\right) \tag{1}$$

$$\Delta E\left(R_{app}, A, E_{app}; f\right) = E_{app}\left(R_{app}, A, E_{app}; f\right) - E_{true}\left(R_{app}, A, E_{app}; f\right) \tag{2}$$

where

$$R_{true} = \text{true range}$$
$$E_{true} = \text{true elevation}$$
$$R_{app} = \text{apparent range}$$
$$E_{app} = \text{apparent elevation}$$

and A is azimuth and f is the frequency under consideration. Pulse dispersion is estimated from the range error at the extremes of the radar pulse bandwidth, specified as:

$$f_{hi} = \text{upper limit of radar bandwidth}$$
$$f_{lo} = \text{lower limit of radar bandwidth}$$

It is calculated as:

$$\Delta t\left(R_{app}, A, E_{app}; \overline{f}\right) = \frac{\left[\Delta R\left(R_{app}, A, E_{app}; f_{lo}\right) - \Delta R\left(R_{app}, A, E_{app}; f_{hi}\right)\right]}{c} \tag{3}$$

27

where $\overline{f} = \frac{1}{2}(f_{lo} + f_{hi})$ and c is the speed of light. The three quantities, ΔR, ΔE, and Δt are written to an output file on a grid of apparent range, azimuth, and apparent elevation for each frequency.

The IDL procedure (actually a set of procedures) reads the IREP specification file and the "radarfreq.dat" control file to obtain the radar characteristics and the nature of the output displays. The user may select either constant altitude displays or constant range displays along with the value of the altitude or range, respectively. An example of the output display is shown in Figure 18.
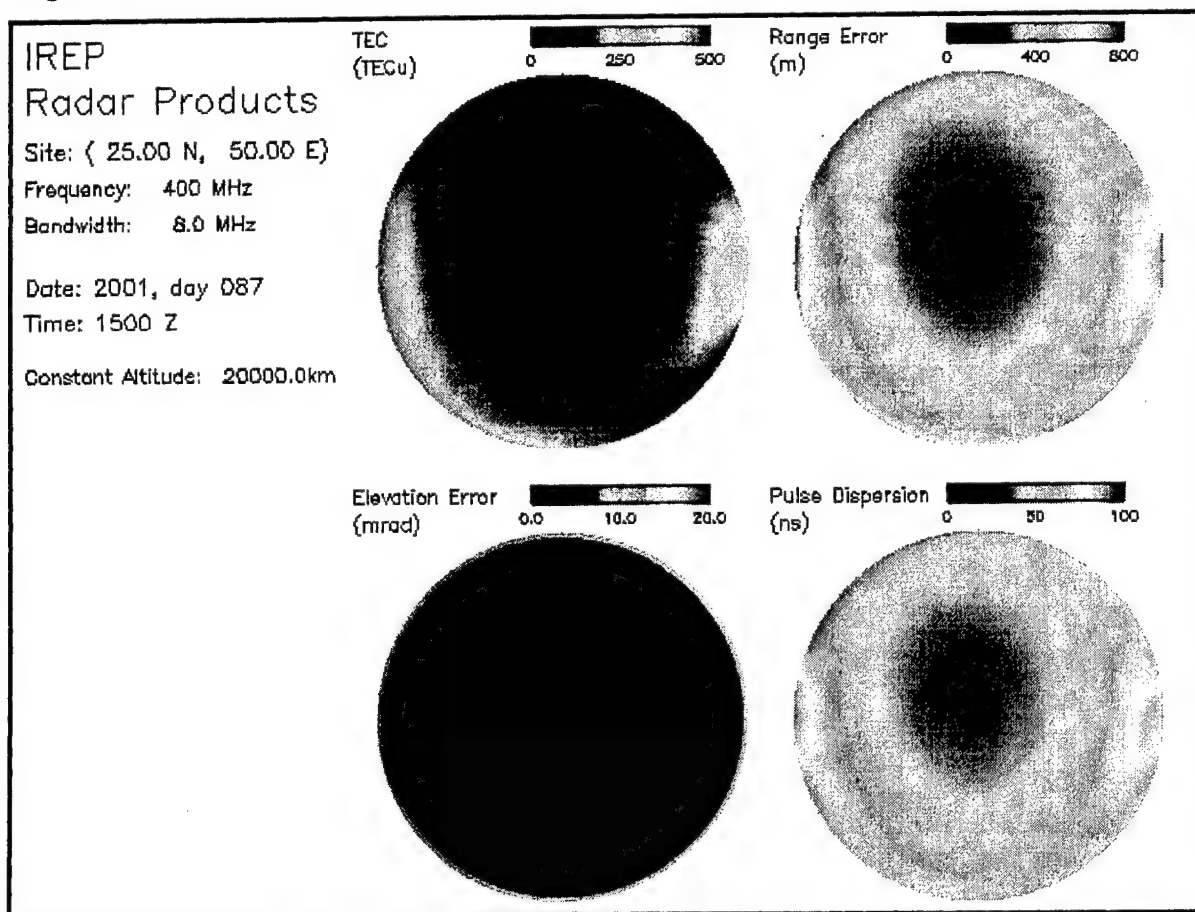
Figure 20. An Example of the IREP Graphical Display for a Hypothetical Radar Sited at (25 N, 50 E) Operating at a Frequency of 400 MHz with a Bandwidth of 8 MHz on 28 March 2001 (day 87) at 1500 UT. The display shows TEC, range error, elevation error, and pulse dispersion. The display is normally in color, but is reproduced here in gray scale.

I installed the four components of IREP on a Linux computer under the control of Dr. Terrance Bullett at AFRL. This computer was running a demonstration version of SEND, including PRISM, on a regular schedule, using data from the DISS network to drive PRISM. The output from PRISM was used by an HF raytracing module in SEND to produce specifications and maps of HF propagation parameters. I set up a script on that computer to run

IREP on a similar schedule, using the same PRISM output files to produce graphical displays of ionospheric radar correction parameters which could be accessed over the AFRL intranet.

3.2 *IRDT*

The second radar related application, actually based on PIM rather than PRISM, is a radar design tool (RDT). The idea for the RDT originated with Mr. Gregory Bishop of AFRL. The overall design of the RDT was developed jointly by Mr. Bishop and me. It currently exists in a preliminary demonstration version, which was delivered to AFRL on CD-ROM.

The IRDT consists of a large database of PIM output files for a variety of climatological conditions and a routine for calculating statistics for a user specified radar site and characteristics. The statistical routine is based on the IREP FORTRAN module, but instead of using a single PRISM output file to produce radar corrections to be displayed graphically, IRDT reads each PIM output file and collects statistics on the ionospheric corrections. User control is provided through control files similar to those used with IREP.

The first IRDT control file is called "radarfreq.dat," which contains information on the radar frequency bands and the nature of the statistics to be accumulated. For this demonstration

```
 2               = NFREQ, the number of radar frequency pairs
 396.0   404.0   = lower limit, upper limit of pulse bandwidth
 990.0 1010.0    = lower limit, upper limit of pulse bandwidth
A                = "A" for constant altitude, "R" for constant range
 20000.0         = altitude or range for accumulation of statistics
0                = statistics regime (0=global, 1=solar activity, 2=seasonal, 3=local time
```

Figure 21. The Radar Control File "radarfreq.dat" Used With IRDT. Although this example specifies only two frequency bands, up to four may be specified. Unlike IREP, IRDT makes use of all the information in this file. This example specifies that statistics are to be accumulated for a constant altitude of 20,000 km under all conditions. The comments (text following the equal sign) are to make the file more readable and easier to edit, but are not required to execute the code.

version of the code, the number of frequency bands is limited to four, but this can be easily increased. The last line in the file is an integer flag that specifies statistics regime.

0   indicates that "global" statistics are to be accumulated. That is, the statistics are to be calculated for all solar activities, seasons, and local times.

1   indicates that statistics are to be calculated separately for each solar activity level (low, moderate, and high) but for all seasons and local times for a given solar activity level. Low solar activity is represented by $F_{10.7} = 70$; moderate, by $F_{10.7} = 130$; and high, by $F_{10.7} = 210$.

2   indicates that statistics are to be calculated for each season (equinox, June solstice, and December solstice) but for all solar activities and local times for a given season. The equinoxes are represented by day 079; June solstice, by day 171; and December solstice, by day 355.

3   indicates that statistics are to be calculated for each local time range (day, night, dawn, dusk) but for all solar activities and seasons for a given local time range. "Night" is taken to be from 2100 to 0300; "dawn", from 0300 to 0900; "day", from 0900-1500, and "dusk", from 1500 to 2100.

For this demonstration version, the statistics that are calculated are the mean and standard deviation of the ionospheric range correction, ionospheric error correction, and the ionospheric pulse dispersion.

The second IRDT control file is called "radargrid.in", and it contains the specification of the azimuth/elevation/range grid use for output. An example is shown in Figure 3.2-2.

```
 25.0,  50.00 :site coordinates: Lat (deg N) REAL[-90.0,90.0], Lon (deg E)  REAL[0.0,360.0)
    20          :Number of elevations INTEGER>0; followed by Elevation grid (deg) REAL[0.0,90.0]
  0.01   1.00   2.00   3.00   4.00   5.00   6.00   7.00   8.00   9.00 10.00 12.00 14.00
 17.00 20.00 25.00 30.00 40.00 60.00 89.99
    37          :Number of azimuths INTEGER>0; followed by Azimuth grid (deg) REAL[0.0,360.0]
   0.00  10.00  20.00  30.00  40.00  50.00  60.00  70.00  80.00  90.00
 100.00 110.00 120.00 130.00 140.00 150.00 160.00 170.00 180.00 190.00
 200.00 210.00 220.00 230.00 240.00 250.00 260.00 270.00 280.00 290.00
 300.00 310.00 320.00 330.00 340.00 350.00 360.00
    67          :Number of alts INTEGER[1,1000]; followed by Alt grid (km) REAL[90.0,25000.0]
   90.00   100.00   125.00   150.00   175.00   200.00   210.00   220.00
  230.00   240.00   250.00   260.00   270.00   280.00   290.00   300.00
  310.00   320.00   330.00   340.00   350.00   360.00   370.00   380.00
  390.00   400.00   410.00   420.00   430.00   440.00   450.00   460.00
  470.00   480.00   490.00   500.00   525.00   550.00   575.00   600.00
  625.00   650.00   675.00   700.00   750.00   800.00   850.00   900.00
  950.00  1000.00  1100.00  1200.00  1300.00  1400.00  1500.00  2000.00
 3000.00  4000.00  5000.00  7500.00 10000.00 12500.00 15000.00 17500.00
20000.00 22500.00 25000.00
```

Figure 22. An Example of the Grid Control File "radargrid.in" That Tells IRDT How to Organize the Output. The user should not ordinarily modify this file. Note the specification of *altitudes* rather than *ranges*, resulting in an elevation dependent range grid. This is done because the ionosphere is horizontally stratified.

The output from IRDT is a rather large text file, in excess of 2000 lines for the global statistics and in excess of 6000 lines for the other statistics options. Therefore, I have supplied an IDL procedure, "plot_irdt.pro" which produces graphical output. An example of the output for the global statistics is shown in Figure 23.
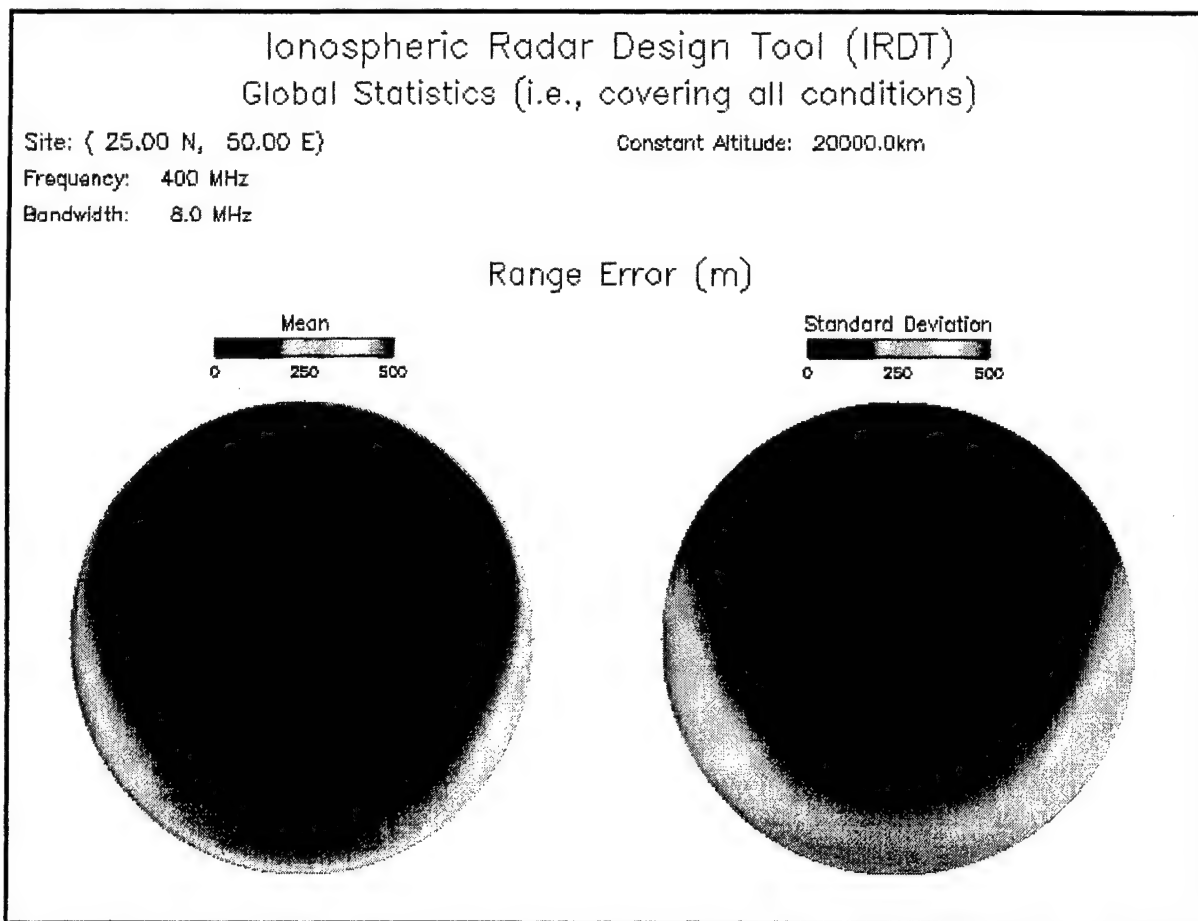
Figure 23. Example of Graphical Output From IRDT and plot_irdt.pro. Here, the overall mean range error (m) is shown in the left panel, while the standard deviation is shown in the right panel. Note that the effect of the Appleton anomaly is visible low on the southeastern and southwestern horizon, with its major impact on the variability. The output is meant to be displayed on a computer screen in color, but is reproduced here in gray scale.

3.3 *Transionospheric Range Delay and Doppler Shift*

With the encouragement and financial support provided by Dr. William Borer of AFRL, Mr. Ray Barnes and I developed application software to facilitate the use of PRISM to calculate radio propagation characteristics for transionospheric applications. Specifically, we developed an IDL procedure to read input data, set up PRISM runs, read the resulting PRISM output files, integrate line-of-sight TEC values, and calculate ionospheric range delay and ionospheric Doppler shift. To facilitate testing, an orbit simulation module was included so that the impact of various satellite orbits could be examined. To facilitate the evaluation of PRISM performance, the plotting software plots the results from PRISM climatology runs, PRISM data assimilation runs, and their differences.

31

Range delay was calculated from [*Klobuchar*, 1985]

$$\Delta R = \frac{40.3 \times 10^4}{f^2} \text{TEC}_{los} \qquad (4)$$

where the transmitter frequency, f, is in MHz and the line of site TEC, TEC_{los}, is in TEC units (10^{16} el m^{-2}), and the range delay, ΔR, is in meters. Ionospheric Doppler shift was calculated from [*Klobuchar*, 1985]

$$\Delta f = \frac{1.34 \times 10^3}{f} \frac{d}{dt} (\text{TEC}_{los}) \qquad (5)$$

with the same units for f and TEC_{los} as for range delay, and the frequency shift, Δf, is in Hz.

To test the software, runs were performed for simulated Low Earth Orbit (LEO), High Earth Orbit (HEO), and Geosynchronous Orbit (GEO) satellites. For the LEO satellite we chose a circular orbit with an inclination of 60° and a period of 90 minutes (corresponding to an altitude of about 283 km). For HEO we selected another circular orbit with an inclination of 60° and a period of 12 hours (corresponding to an altitude of about 20,300 km). Finally, for GEO we selected an equatorial circular orbit with a period of 24 hours (corresponding to an altitude of approximately 35,900 km). In addition, we fixed the simulated transmitter at (45.44°N,12.32°E) and 60 MHz.

Dr. Borer obtained data from JPL from a network of GPS receivers in Europe for two non-consecutive days: 24 and 26 October 2002. The slant TEC values were converted to vertical equivalent TEC for ingestion into PRISM, and several data sets were derived by applying various time windows and elevation masks. Specifically, the high elevation files included only the five highest elevation observations from each station. However, a few of the stations provided fewer than five observations, so they are underweighted compared to the other stations. We considered the possibility of adding interpolated values, or otherwise artificially increasing the number of observations for the underweighted stations, but decided that this really required a separate investigation to determine the best method for handling this problem. The results presented below are for the data as provided.

Table 10. TEC Data File List for Transionospheric Propagation Calculations.

File name	Date	Time Window (UT)	Elevation Mask
all_time_0.tec	24 October 2002 (day 297)	0548-0803	None
narrow_time_all_0.tec	"	0643-0705	None
narrow_time_high_el_0.tec	"	0643-0705	5 highest
all_time_1.tec	26 October 2002 (day 299)	0420-0631	None
narrow_time_all_1.tec	"	0514-0536	None
narrow_time_high_el_1.tec	"	0514-0536	5 highest

Figure 24 gives the results for the full data sets for 24 October 2002, respectively for the simulated GEO satellite. For this case, in which the satellite is stationary relative to the transmitter, the variability of the range delay and Doppler Shift are due entirely to ionospheric variability. Not surprisingly, the ionospheric Doppler shift is so small that it is undetectable at the transmitter frequency.

Transmitter location = (45.44N, 12.32E), frequency = 60.0 MHz; Satellite Orbit = GEO
Start date & time: 2002.10.24 0550 UT (all_time)
PRISM grid spacing: 1.0° lat, 1.0° lon; PRISM run interval: 5 min
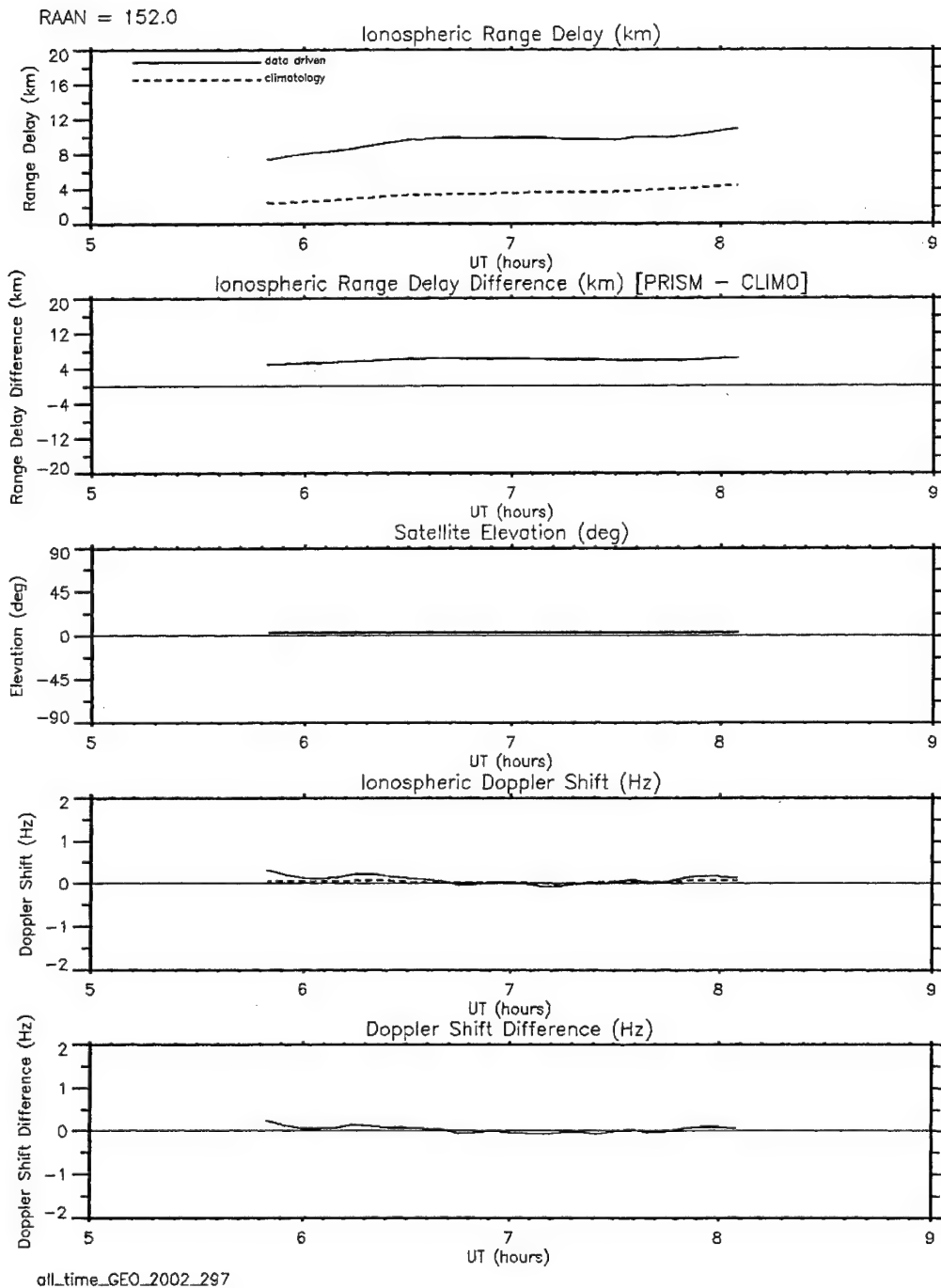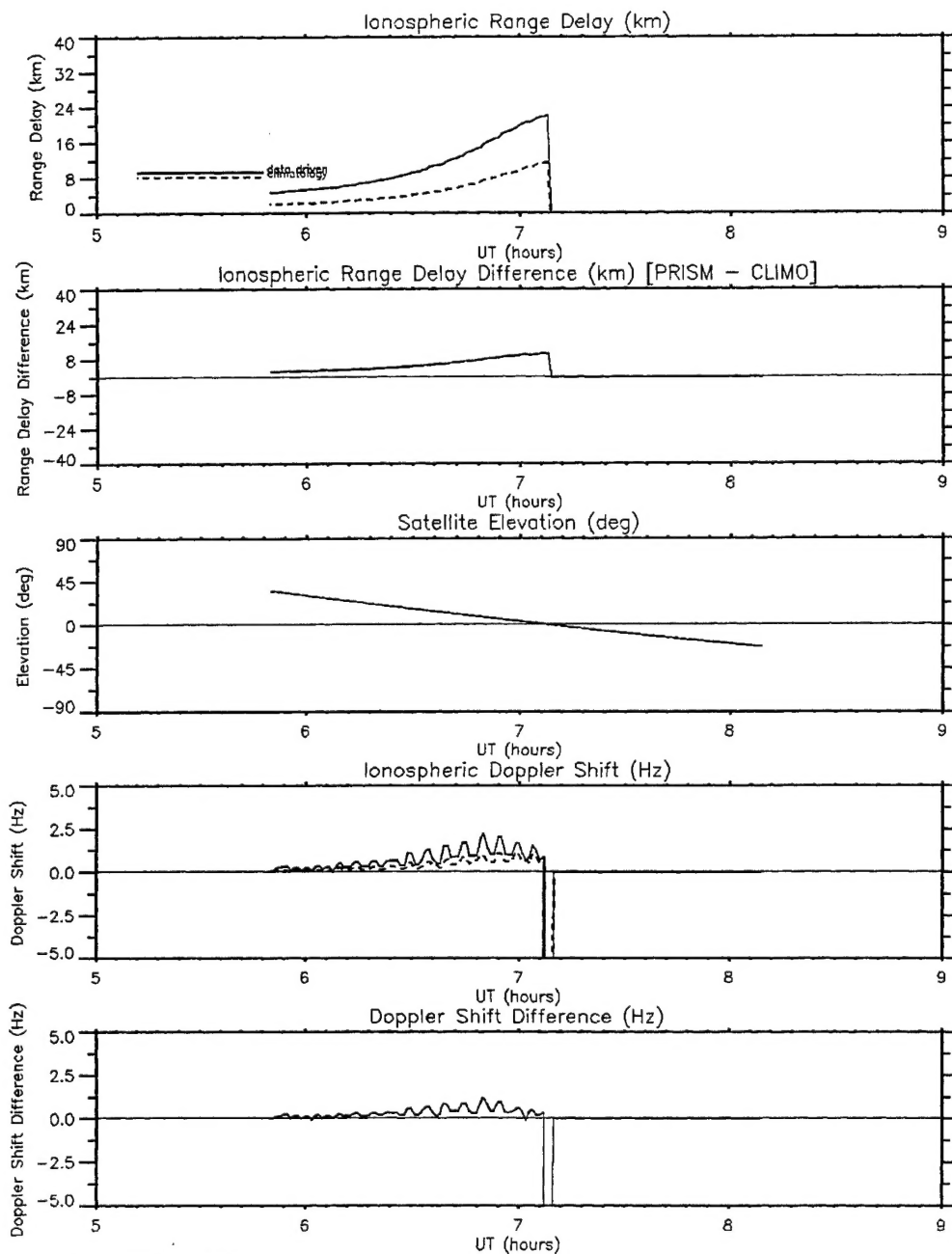satellite position interval: 300 sec

all_time_GEO_2002_297

Figure 24. Comparison of PRISM Climatology and Data Assimilation Runs for 24 October 2002 Using the Full Data Set Supplied by Dr. Borer and a Simulated GEO Satellite. The top panel shows range delay from PRISM climatology (dashed) and PRISM data assimilation (solid). The next panel shows the difference between the two. The middle panel shows the satellite elevation, which is constant in this case. The next panel shows the ionospheric contribution to the Doppler shift for climatology and data assimilation. Finally the bottom panel shows the difference between the two.

33

Figures 25 and 26 on the following pages show similar results for the simulated HEO and LEO satellites, respectively. Here, because the ionospheric Doppler shift is estimated using numerical differences, it becomes unrealistically large as the satellite appears and disappears over the horizon. Some effort should be put into correcting this problem in the future.

We are not sure what causes the interesting periodic structure in the Doppler shift plot for the HEO satellite. It probably has to do with the difference in the rate at which PRISM is updated and the rate at which the satellite position is updated. For all three plots we ran PRISM at 5 minute intervals, whereas we calculated the satellite position at 5 second intervals for LEO, 1 minute intervals for HEO, and 5 minute intervals for GEO. Because the PRISM rate and satellite position update interval are the same for GEO no effect is seen there. The effect is obscured by the choice of vertical scale in the LEO plot, but appears to be there as well. We anticipated some sort of sawtooth effect due to the relatively long PRISM update interval, so we do not know whether the relative smooth nature of the curve in the figures may be an artifact of the plotting software. This should also be investigated in the future.

Transmitter location = (45.44N, 12.32E), frequency = 60.0 MHz; Satellite Orbit = HEO
Start date & time: 2002.10.24 0550 UT (all_time)
PRISM grid spacing: 1.0° lat, 1.0° lon; PRISM run interval: 5 min
satellite position interval: 60 sec

all_time_HEO_2002_297

Figure 25. Comparison of PRISM Climatology and Data Assimilation Runs for 24 October 2002 Using the Full Data Set Supplied by Dr. Borer and a Simulated HEO Satellite. The top panel shows range delay from PRISM climatology (dashed) and PRISM data assimilation (solid). The next panel shows the difference between the two. The middle panel shows the satellite elevation, which shows that the satellite passed below the horizon shortly after 0700 UT. The next panel shows the ionospheric contribution to the Doppler shift for climatology and data assimilation. Finally the bottom panel shows the difference between the two.
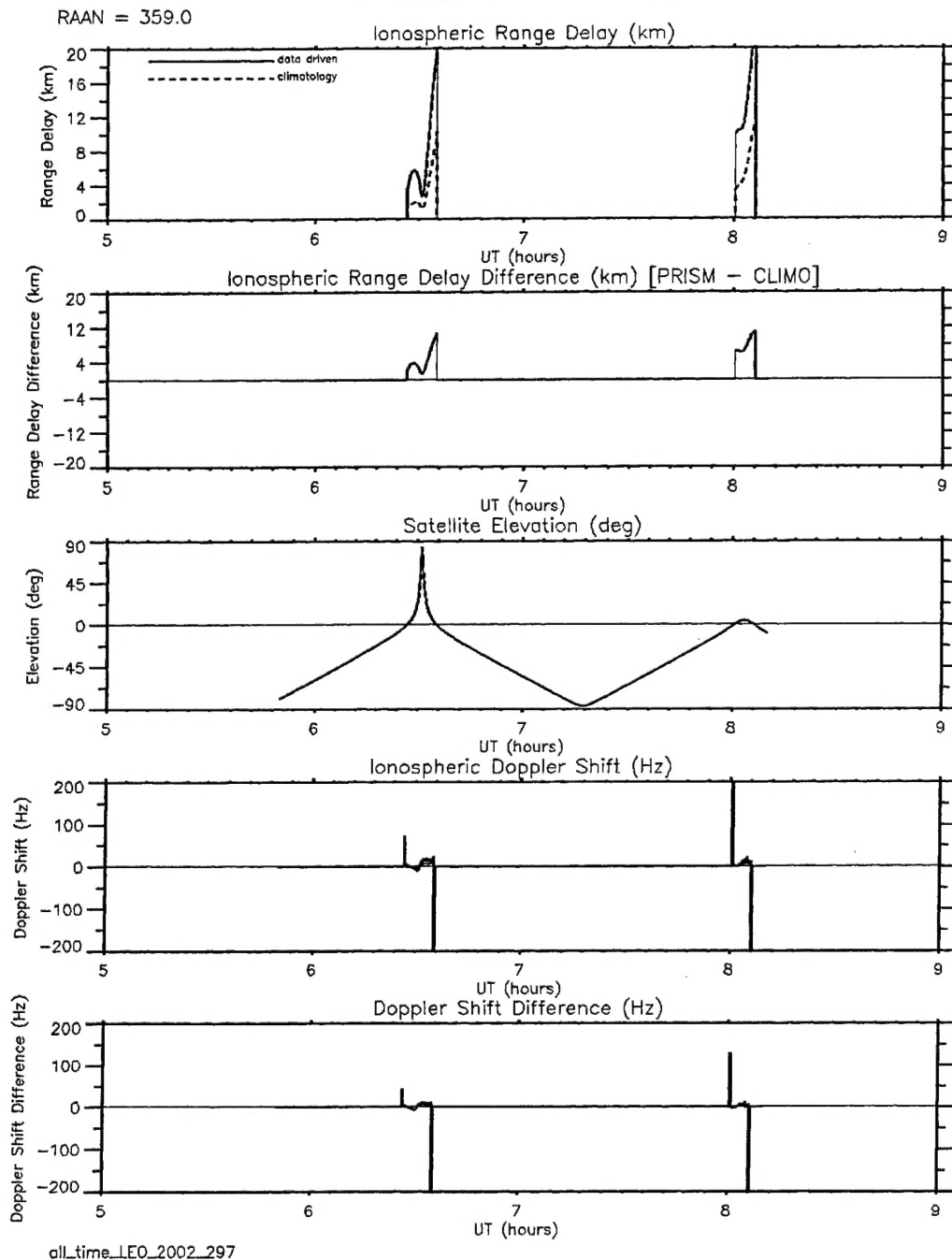
35

Figure 26. Comparison of PRISM Climatology and Data Assimilation Runs for 24 October 2002 Using the Full Data Set Supplied by Dr. Borer and a Simulated LEO satellite. The top panel shows range delay from PRISM climatology (dashed) and PRISM data assimilation (solid). The next panel shows the difference between the two. The middle panel shows the satellite elevation, which shows that the satellite spent most of its time below the horizon. The next panel shows the ionospheric contribution to the Doppler shift for climatology and data assimilation. Finally the bottom panel shows the difference between the two.

36

References

Klobuchar, J. A., Ionospheric Time Delay Effects on Earth-Space Propagation, in *Handbook of Geophysics and the Space Environment*, (NTIS document accession number ADA 167000), pp. 10-84 – 10-88, 1985.